View Online

What do we need for a superhydrophobic surface? A review on the recent progress in the preparation of superhydrophobic surfaces

Xue-Mei Li, David Reinhoudt* and Mercedes Crego-Calama*

Received 17th October 2006
First published as an Advance Article on the web 31st January 2007
DOI: 10.1039/b602486f

Superhydrophobic surfaces have drawn a lot of interest both in academia and in industry because of the self-cleaning properties. This *critical review* focuses on the recent progress (within the last three years) in the preparation, theoretical modeling, and applications of superhydrophobic surfaces. The preparation approaches are reviewed according to categorized approaches such as bottom-up, top-down, and combination approaches. The advantages and limitations of each strategy are summarized and compared. Progress in theoretical modeling of surface design and wettability behavior focuses on the transition state of superhydrophobic surfaces and the role of the roughness factor. Finally, the problems/obstacles related to applicability of superhydrophobic surfaces in real life are addressed. This review should be of interest to students and scientists interested specifically in superhydrophobic surfaces but also to scientists and industries focused in material chemistry in general.

Published on 31 January 2007 on http://pubs.rsc.org | doi:10.1039/B602486F
Downloaded on 29 November 2010

1 Introduction

Wettability of a solid surface is an important property[1–4] because controlling the surface wettability is crucial in many practical applications.[5,6] A direct expression of the wettability of a surface is the contact angle (CA) of a water droplet on the surface. Surfaces with very high water contact angles particularly larger than 150° are usually called superhydrophobic (SH) surfaces. These surfaces are of special interest, because properties such as antisticking, anti-contamination,[7,8] and self-cleaning[9–13] are expected. These properties are desirable for many industrial and biological applications such

Laboratory of Supramolecular Chemistry and Technology group, MESA+ Institute for Nanotechnology, University of Twente, P. O. Box 217, 7500AE, Enschede, The Netherlands

Xue-Mei Li

Dr. Xue-Mei Li was born in China in 1971. She received her Bachelor degree of Engineering at Dalian University of Technology in 1994. Thereafter, she was admitted by Dalian Institute of Chemical Physics, Chinese Academy of Sciences (CAS) and received her master degree in 1997. In 1998, she moved to the Netherlands, and started to work at Prof. Reinhoudt's group for a short project. Meanwhile, she was offered a PhD candidateship. In 2003, she obtained her PhD degree in nanofabrication. In 2004, she started her career at DSM Resins BV working at the Customer Competence Center in Zwolle. One year later, she came back to University of Twente and joined Prof. Reinhoudt as a post-doctoral researcher working on the development of superhydrophobic surfaces for medical applications. Her PhD thesis was awarded the Backer prize in 2004. Her research interest encompasses nanolmicrofabrication, development of nanomaterials, and application of nanotechnology in medicine.

David N. Reinhoudt

Professor David N. Reinhoudt was born in 1942 in The Netherlands. He studied Chemical Technology at the Delft University of Technology and graduated (suma cum laude) in chemistry in 1969 with Professor H. C. Beijerman. In the period 1970–1975 he worked at Shell where he started the crown ether research program. In 1975 he was appointed as a part-time professor (extraordinarius) at the University of Twente followed by the appointment as a full professor in 1978. The major part of his research deals with supramolecular chemistry and technology. Nanotechnology, molecular recognition, and non-covalent combinatorial synthesis are the major fields. His interest is also on application of supramolecular chemistry e.g. in ''lab-on-a-chip'', in the field of electronic or optical sensor systems, catalysis, and molecular materials. Prof. Reinhoudt is the scientific director of the MESA$^+$ Research Institute. Since 2002 he is the chairman of the Board of NanoNed, the Dutch Network for Nanotechnology. He is a member of the Royal Dutch Academy of Sciences, Fellow of the American Association for the Advancement of Science, and Fellow of the Institute of Physics. He is the author of more than 800 scientific publications, patents, review articles, and books. He has been honored with the Izatt–Christensen award (1995), the Simon Stevin Mastership (1998) and Knight of the Order of the Dutch Lion (2002).

 This journal is © The Royal Society of Chemistry 2007

View Online

Published on 31 January 2007 on http://pubs.rsc.org | doi:10.1039/B602486F
Downloaded on 29 November 2010

as antibiofouling paints for boats,[14,15] antisticking of snow for antennas and windows,[16,17] self-cleaning windshields for automobiles,[18] metal refining, stain resistant textiles, antisoiling architectural coatings.[19] The wettability of a surface is directly related to the surface energy. Materials with low surface energy, for example a surface with hexagonally packed $-CF_3$ groups gives water contact angles as high as 120°.[20,21] These surfaces are easy to clean, however, they do not have self-cleaning properties. In nature, many natural species exhibit water contact angle higher than 150° such as sacred lotus leaves,[4] water strider's legs,[22] cicada orni's wings,[23] *etc.* These surfaces are water repellent in that the water droplets roll off the surface at a small tilt angle (sliding angle) and hereby removing contaminates from the surface (self-cleaning).

Recently, a great deal of research has been devoted to the preparation and theoretical modeling of superhydrophobic surfaces as witnessed by the large number of publications and diverse approaches.[3,4,24–26] The major objective of this review is: (a) to discuss the superhydrophobic effect and self-cleaning mechanism; (b) to illustrate the most recent progress in the preparation methods in a systematic way; (c) to address the potential application of superhydrophobic coatings, and (d) to review a series of theoretical models in order to provide guidelines for the preparation of superhydrophobic surfaces. Because water repellency mechanisms, self-cleaning materials, and application potentials have been reviewed in a number of publications,[3,4,26] here we only give an overview of the most recent activities (the last three years) in this area. The major part of this review is organized in five sections. The first section gives a brief introduction about the superhydrophobic effect. The second section briefly summarizes the basic guidelines for the preparation of superhydrophobic surfaces and the characteristics of natural superhydrophobic surfaces. The third section provides a comprehensive overview on the strategies for the preparation of superhydrophobic surfaces, with special focus on the fabrication methodology, materials, and structures. The fourth section discusses the recent progress in theoretical modeling, while the fifth section gives an overview of the potential application of superhydrophobic surfaces. Finally a personal perspective of the principles of fabrication of superhydrophobic surfaces is given.

Mercedes Crego Calama

Dr. Mercedes Crego Calama was born in Salamanca, Spain in 1967. Here, she received her Master degree (1991) and her PhD (cum laude) in Chemistry (1995) with J. R. Moran. In 1995, she moved to University of Pittsburgh, USA (NATO fellowship) to collaborate with A. D. Hamilton. In 1997 she was awarded with a Marie Curie European postdoctoral fellowship and she moved to the University of Twente, The Netherlands where she worked with D. N. Reinhoudt on dynamic combinatorial libraries. In 2000, she became Researcher of the Royal Dutch Academy of Sciences (KNWA) working on combinatorial sensor fabrication. Alongside her KNWA duties, she currently holds a tenured position as Universiteit Docent in the University of Twente. Her current research interests, besides in glass microarrays, are in the design and fabrication of nanostructures via self-assembly and self-organization.

2 Theoretical background and characteristics of natural species

2.1 Theoretical background

The wettability of a flat surface, expressed by contact angle (CA) θ of a water droplet, is given by Young's equation:

$$\cos\theta = \frac{\gamma_{SV} - \gamma_{SL}}{\gamma_{LV}} \quad (1)$$

where γ_{SV}, $\gamma_{SL}$and γ_{LV} refer to the interfacial surface tensions with S, L, and V as solid, liquid, and gas, respectively. Young's angle is a result of thermodynamic equilibrium of the free energy at the solid–liquid–vapor interphase.

Depending on the value of the contact angle, surface properties are determined as hydrophobic (CA $>$ 90°) or hydrophilic (CA $<$ 90°). In practice, two types of CA values are used: static and dynamic CAs. For a flat surface, static contact angle is close to Young's angle. Dynamic contact angles are non-equilibrium CAs. Static CAs are obtained by sessile drop measurements, where a drop is deposited on the surface and the value is obtained by a goniometer. Dynamic CAs are measured during the growth (advancing CA, θ_a) and shrinkage (receding CA, θ_r) of a water droplet. The difference between θ_a and θ_r is defined as contact angle hysteresis ($\Delta\theta$). The values of $\Delta\theta$ can be as low as 10° for a self-assembled monolayer on silicon, and many surfaces show much larger hysteresis due to chemical heterogeneity and roughness.[27,28]

Surfaces with water CA higher than 150° are superhydrophobic or ultraphobic (with very little CA hysteresis). This very high CA is normally called apparent CA since this value does not represent the "real" CA value of the corresponding flat surfaces. The superhydrophobic surfaces are usually covered with micro- or nanoscale asperities (rough). The behavior a water droplet on a rough surface is schematically shown in Fig. 1. Water can either penetrate the asperities or suspend above the asperities. In either case, much higher contact angles are observed than that obtained for the corresponding flat surface. These two situations are named the Wenzel state (penetration) and the Cassie–Baxter state (suspension) after the corresponding theoretical models: the Wenzel[29] and Cassie–Baxter (CB)[30] models. These models

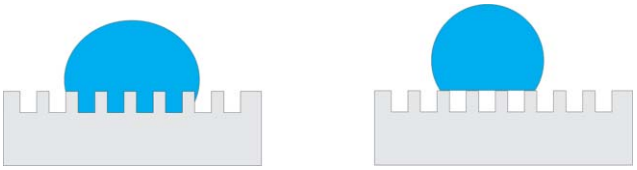

Fig. 1 Behavior of a liquid drop on a rough surface. Left, liquid penetrates into the spikes (Wenzel state); right: liquid suspends on the spikes (Cassie–Baxter state).

View Online

Published on 31 January 2007 on http://pubs.rsc.org | doi:10.1039/B602486F
Downloaded on 29 November 2010

form the basic guidelines for the study of superhydrophobic surfaces.[11,31–36]

The basic assumption in Wenzel's theory is that the liquid follows the roughness of the surface as shown in Fig. 1 (left). At thermodynamic equilibrium, there is a linear relationship between the apparent contact angle of the surface and the roughness factor of the given surface:

$$\cos \theta^{w} = r \cos \theta \quad (2)$$

where θ^{w} corresponds to the apparent contact angle, r represents the roughness factor, and θ refers to Young's angle.

The roughness factor is defined by the actual surface area divided by the projected surface area, therefore, for a rough surface $r > 1$. Following Wenzel's prediction, for a hydrophobic surface $\theta^{w} > \theta > 90^{\circ}$ and for a hydrophilic surface $\theta^{w} < \theta < 90^{\circ}$. Roughness enhances both hydrophobicity and hydrophilicity depending on the nature of the corresponding flat surface.[24] In the Wenzel's regime, the contact angle and its hysteresis increases as the roughness factor increases for a hydrophobic surface. Nevertheless, it has been demonstrated that the contact angle increases steadily with the roughness factor until it exceeds 1.7 then contrary to the Wenzel's prediction the contact angle hysteresis starts to decrease.[37,38] The decrease in the contact angle hysteresis is attributed to the switching from the Wenzel to the Cassie–Baxter state because of the increased air fraction leading to the suspension of water droplet on top of the asperities as shown in Fig. 1, right. The suspension of water droplet is also described as a composite state.

As a result of the suspension of the water droplet on the asperities, in the Cassie–Baxter (CB) model,[30] the apparent contact angle is the sum of all the contributions of the different phases as described by eqn (3):

$$\cos \theta^{c} = f_1 \cos \theta_1 + f_2 \cos \theta_1 \quad (3)$$

where θ^{c} is the apparent CA, f_1 and f_2 surface fraction of phase 1 and 2, respectively; θ_1 and θ_2 CA of phase 1 and phase 2, respectively. For a rough surface containing only one type of asperities, given f is the solid fraction, then the air fraction is $(1 - f)$. With $\theta = 180^{\circ}$ for air, the resulting CA can be calculated by the following equation:

$$\cos \theta^{c} = f(1 + \cos \theta) - 1 \quad (4)$$

Thus, for the CB model, the apparent CA (θ^{c}) is a sole function of solid fraction for a given surface with CA θ. Therefore, to obtain a superhydrophobic surface, the contribution of the solid part should be as small as possible or a solid material with very high CA should be used. In practice, the CB model cannot predict accurately the wetting behavior of a predesigned surface. However, it is often used to compare it with a practical result in order to confirm the presence of the CB state.

In summary, both theories can predict the contact angle of a rough surface only qualitatively. Furthermore, it is not evident which theory should be used and when. Therefore, it would be very important to obtain some guidelines for predicting the surfaces behavior, which is critical in designing superhydrophobic surfaces. Thus, many research interests have been devoted to modeling superhydrophobic surfaces. The new models for predicting surface wettability will be discussed in more detail in section 4.

2.2 Structures of natural superhydrophobic (SH) surfaces

Many plant surfaces[39] and animal furs[22] exhibit water repellent properties, *i.e.* very high water CA. With the aid of scanning electron microscopy (SEM), the microstructures of plant surfaces have revealed that water repellency is mainly caused by epicuticular wax crystalloids that cover the cuticular surface in a regular microrelief of about 1–5 μm in height.[40,41]

Lotus leaves are one of the most famous examples among naturally occurring superhydrophobic surfaces.[7] The water CA of a lotus leaf is 161 ± 2.7° with CA hysteresis of 2°.[4,42] Pictures of a lotus leaf and its microstructure image obtained by Barthlott and Neihuis are shown in Fig. 2. The structure of a lotus leaf consists of a combination of a two scale roughness: one around 10 μm (rough structure) and one around 100 nm (fine structure). These surfaces are also referred as hierarchical micro- and nano-structures.[4] The hydrophobicity of a lotus leaf arises from the epicuticular wax secreted by the leaf itself.[7] The wax has a contact angle of 110°, not highly hydrophobic, however, the lotus leaf still exhibits a superhydrophobic property. It is presumed that this combination of roughness and wax contribute to the superhydrophobicity of the lotus leaf[4,42] The rolling off of water droplets and collecting the contaminants from the lotus leaf is dubbed as the "lotus effect". The lotus leaf therefore always exhibits a very low degree of contamination: self-cleaning.

The self-cleaning effect is evident for the lotus leaf. The underlying mechanism has been thoroughly studied. At the interface between a viscous fluid and a solid surface, usually, a nonslip boundary condition dominates.[43] Slip on the boundary can occur on the scale of a few tens of nanometers, which is not appreciated for macroscopic flow. However, when a drop moves down a tilted rough SH surface, due to the high contact angle (minimized contact between the fluid and surface), effective macroscopic slip occurs on scales consistent with the characteristic size of the surface features. For a drop of water rolling off a lotus leaf, the droplet behaves as an elastic ball

Fig. 2 A microscopic SEM image of a lotus leaf showing the two-scale roughness. (Picture adapted from ref. 7 with kind permission of Springer Science and Business Media.)

 This journal is © The Royal Society of Chemistry 2007

View Online

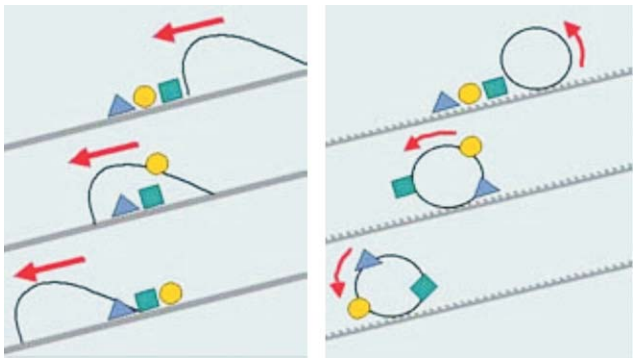

Fig. 3 Slip of a water droplet from an inclined hydrophobic surface (left) where the water drop crawls over the dust particles and an inclined superhydrophobic surface (right) where the dust particles are collected and taken away: self-cleaning. (Pictures adapted from ref. 7, with kind permission of Springer Science and Business Media.)

rather than a fluid (Fig. 3). In case of a normal hydrophobic surface, because of the nonslip boundary condition, the water drop falls across the dirt particles and the dirt particles are mainly displaced to the sides of the droplet and re-deposited behind the droplet. Especially hydrophobic particles tend to remain on such surfaces (Fig. 3, left). In the case of water-repellent rough surfaces, the solid/water interface is minimized. Water forms a spherical droplet, and collects the particles from the surface (Fig. 3, right). The rolling off of water droplets and collecting the contaminants from the lotus leaf is dubbed as the "lotus effect". The lotus leaf therefore always exhibits a very low degree of contamination: self-cleaning.

In animals, water repellent structures are also quite common.[23] Recently Jiang *et al.* have reported that a water strider's leg contains hierarchical micro- and nanostructures.[22] They ascribe the water strider's capability of standing and moving rapidly on water to numerous oriented, needle-shaped setae on the legs (Fig. 4). The setae are needle-shaped, with diameters ranging from 3 microns down to several hundred nanometers. Most setae are roughly 50 μm in length and arranged at an inclined angle about 20° from the surface of the leg. Many elaborate, nanoscale grooves are evident on each microseta forming a unique hierarchical structure. The maximal supporting force for a single leg is about 15 times of the body weight of a water strider before it will pierce into the water as tested by using a cantilever made of a water strider' leg. This phenomenon is ascribed to super water repellency of the hierarchical structures of the legs.

3 Methods used for the preparation of superhydrophobic surfaces

Both Wenzel and Cassie–Baxter theories have pointed out that a rough surface is essential for enhancing hydrophobicity and hydrophilicity. In practice, the approaches for superhydrophobic surface preparation can be basically categorized into two directions: top-down and bottom-up approaches. Top-down approaches encompass lithographic and template-based techniques,[43] and plasma treatment of the surfaces.[32,34,36,44–51] Bottom-up approaches involve mostly self-assembly and self-organization.[43,52–60] Examples of bottom-up approaches include chemical deposition,[60–66] layer-by-layer (LBL) deposition,[52,53,57,60,62] hydrogen bonding,[67] and colloidal assemblies.[35,43,59,68–70] There are also methods based on the combination of both bottom-up and top-down approaches, for example, casting of polymer solution and phase separation,[71] and electrospinning.[63,72–74] In the following section, different approaches are addressed in detail.

3.1 Top-down approaches

Top-down approach is a general term in microelectronics referring to the fabrication of materials and devices by carving, molding, or machining bulk materials with tools and lasers. For the generation of superhydrophobic surfaces, template[75,76] and lithographic approaches,[10,33,77–80] micromachining,[31] and plasma treatments have been used. Templation often involves molding and replication steps. Thereafter, the template can be removed by lifting off[75,76] or dissolution[81] or even sublimation.[82,83] In the lithographic approaches, light is irradiated through a mask with desired features onto the substrates (often silicon) with a photoresist. Subsequent etching steps yield the desired patterned surfaces. These surfaces are made hydrophobic by silanization.[10,33,77–80] In micromachining, surfaces are diced into the desired texture.[31] In the plasma treatments, surfaces are etched anisotropically thus generating rough surfaces. Examples includes plasma treatment of poly(ethylene terephthalate) (PET),[49,50] poly(tetrafluoroethylene) (PTFE),[84] and polyethylene (PE).[44] Pulse-laser treatments of poly-(dimethylsiloxane) (PDMS) for the generation of superhydrophobic surfaces have also been shown.[85,86]

3.1.1 Templation. Templation involves the use of a master with the desired features, replication of the features (Fig. 5) by molding and subsequent lifting off the replica or dissolution of the templates. Templation is useful for the preparation of

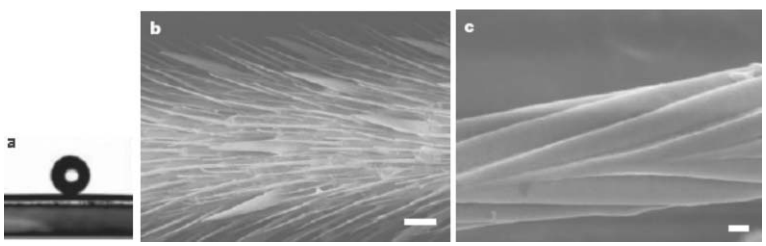

Fig. 4 Images of the non-wetting leg of a water strider. (a) a water droplet on a leg with a contact angle of 167.6 ± 4.4°; (b) and (c), scanning electron microscope images of the leg showing numerous oriented spindly microsetae (b) and the fine nanoscale grooved structures on a seta (c). Scale bars: (b) 20 μm, (c) 200 nm. (Reprinted with permission from Macmillan Publishers Ltd: [Nature].[22] Copyright 2004.)

Published on 31 January 2007 on http://pubs.rsc.org | doi:10.1039/B602486F
Downloaded on 29 November 2010

View Online

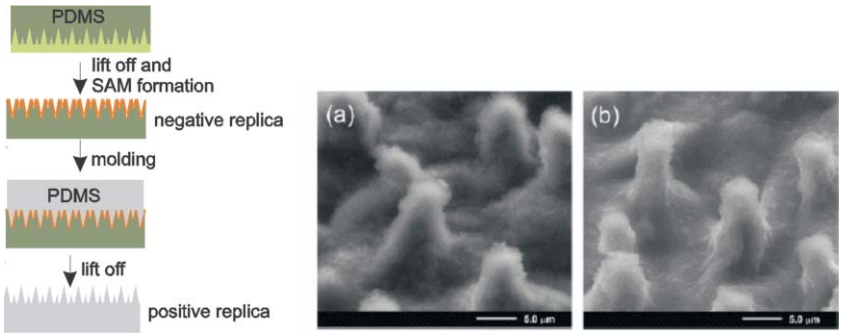

Fig. 5 Schematic illustration of nanocasting and SEM images of (a) a natural lotus leaf and (b) its positive PDMS replica. (Images reprinted with permission from Sun *et al.*[42] Copyright 2005, American Chemical Society.)

Published on 31 January 2007 on http://pubs.rsc.org | doi:10.1039/B602486F
Downloaded on 29 November 2010

polymeric superhydrophobic coatings. Many materials can be used as a template ranging from natural lotus leaves,[42] a master prepared by lithographic processes, to commercial inorganic membranes.

Sun *et al.*[42] have used a lotus leaf as the template, where the replication process was denoted nanocasting. After casting and lifting off PDMS, a negative replication of the lotus leaf structure was obtained (Fig. 5). This negative template was used further as a master for preparation of a positive replica of the lotus leaf. The positive replica has almost the same surface morphology on both the micro- and nanoscale as the natural lotus leaf. The SEM images of the positive replica showed small papillae hills with an average distance of 6 microns. Even the intricate nanotextures between the hills and in the valleys were clearly replicated (Fig. 5, SEM images). The positive replica exhibits the same superhydrobic property as the natural lotus leaf with an advancing contact angle of 160°. On the other hand the negative replica of the lotus leaf has a contact angle of 110°.

In a similar replication process He *et al.*[76] have fabricated PDMS structures with features of relatively big size (squared posts of 25 microns in width, 30 microns in depth, at varied distances from 8 to 80 microns). The replication process was based on a master prepared by macromachining. A water drop can both be suspended on top of the posts and wet the posts depending on how the water drop is deposited. In case of gentle deposition, a composite form is formed, and the observed contact angles are close to the CB theory prediction. When the water is dropped from some height, the gaps between the posts were wetted and the measured apparent contact angle follows the Wenzel theory (Fig. 6).

Nanoimprint lithography is also a pattern replication process, however, the pattern replication is accomplished by heat- and pressure-driven process where a hard master is pressed onto a thermoplastic polymer layer above the glass transition temperature of the polymer.[87] After cooling and removing the master a negative replica of the template is obtained. Nanoimprint lithography is capable of making very small features down to a few nanometers depending on the master design.

Lee *et al.*[23] have demonstrated the use of nanoimprint lithography for the preparation of polystyrene substrates with different nanostructures as shown in Fig. 7. Textured aluminium sheets and anodic aluminium oxide (AAO)

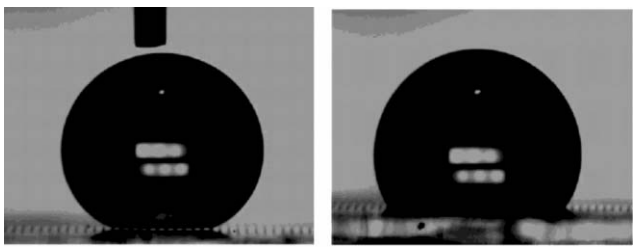

Fig. 6 Direct observation of a composite drop and a wetted situation on the surface depending on how the drop is deposited on the surface. Left, gentle deposition (suspension); right, water drop deposited from a distance (collapsed). (Images reprinted with permission from He *et al.*[76] Copyright 2003, American Chemical Society.)

membranes were prepared and used as replication templates. Polystyrene (PS) polymer substrates were applied in the nanoimprinting process. After cooling down to room temperature and pressure release, the replication template was removed from the polymer substrate by dissolution of Al with saturated $HgCl_2$ solution to give the large area, nanostructured PS surface. The diameters of PS nanofibers were controlled by using the AAO replication templates with different pore

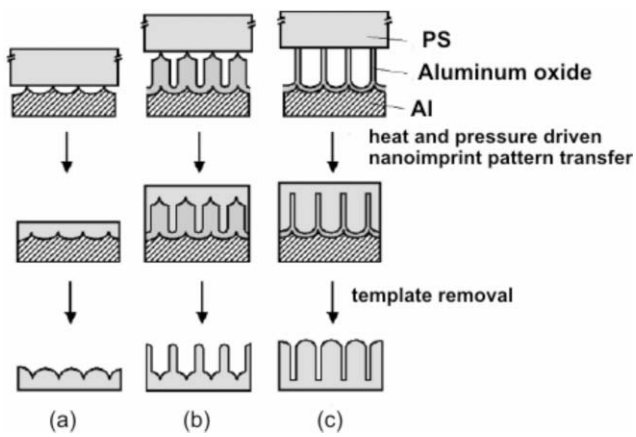

Fig. 7 Schematic outline of the heat- and pressure-driven nanoimprint pattern transfer process for nanofabricating the surface of the thick polymer substrate with (a) aligned nanoemboss, (b) nanopost array with embossed base, and (c) aligned nanofibers. (Images reprinted with permission from Lee *et al.*[23] Copyright 2004, American Chemical Society.)

 This journal is © The Royal Society of Chemistry 2007

View Online

Published on 31 January 2007 on http://pubs.rsc.org | doi:10.1039/B602486F
Downloaded on 29 November 2010

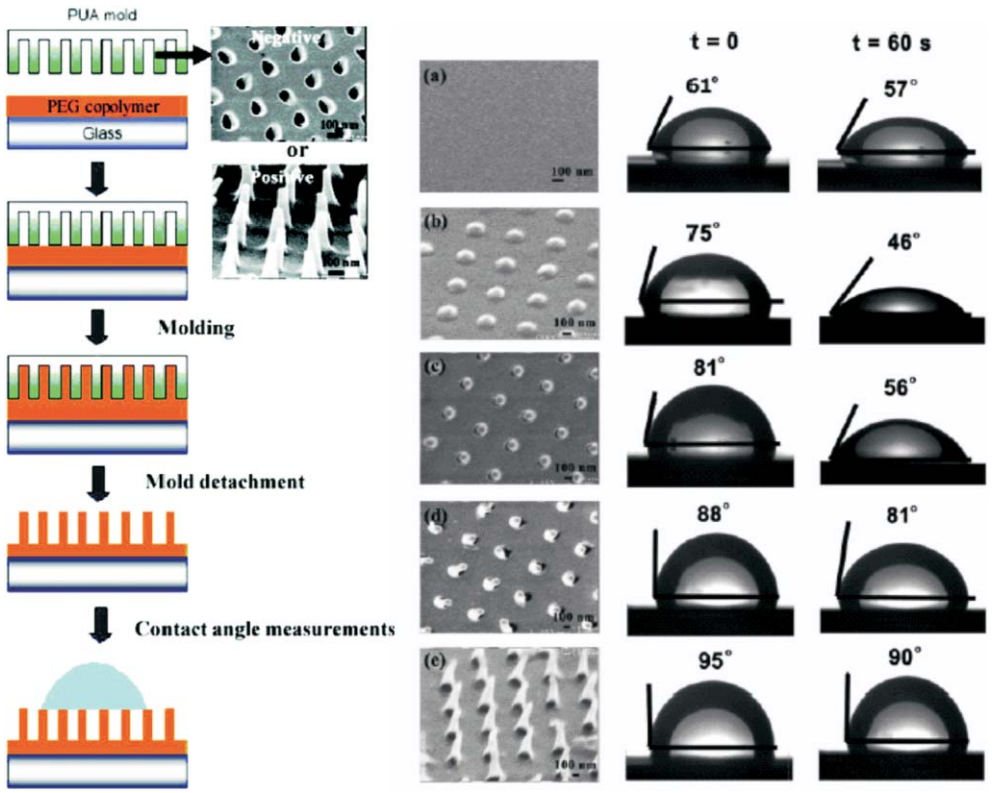

Fig. 8 Schematic illustration of the capillary lithography, tilted SEM images for various PEG copolymer nanostructures with a negative PUA mold, and the corresponding contact angles of water with time at $t = 0$ and 60 s.[75] (a) the bare PEG; (b), (c), (d) and (e) with a pillar height of 170, 310, 440 and 500 nm, respectively. (Images reprinted with permission from Suh *et al.*[75] Copyright 2005. American Chemical Society.)

diameters; the pore diameter was adjusted to the desired dimension by wet-chemical etching. On the other hand, the length of PS nanofibers could be controlled by appropriately varying the thickness of the AAO template. The resultant surfaces showed water CA between 155.8 (1.1°) and 147.6 (1.9°). A water drop placed on the surface rolls easily on the horizontal surface upon slight tilting, reflecting the high degree of water-repellent surface property.

Unlike imprint nanolithography, capillary force lithography involves a patterned elastomeric mold instead of a hard master, where the mold is directly laid onto a spin coated polymer film on a substrate (Fig. 8). The negative replica of the mold is formed by raising the temperature above the polymer's glass transition temperature after solvent evaporation (temperature-induced capillarity) or by direct molding prior to solvent evaporation (solvent induced capillarity).

Suh and Jon[75] have demonstrated the use of capillary lithography for the preparation of poly(ethylene glycol) (PEG) structures with controllable wettability by changing the geometry of the nanostructures. PEG nanostructures were prepared by the use of an ultraviolet (UV) curable mold consisting of functionalized polyurethane with acrylate group. Two distinct wetting states were observed depending on the height of the nanostructures. The feature size, initial contact angles, and equilibrium contact angles of the surfaces are shown in Table 1. A flat PEG surface is relatively hydrophilic with an initial water contact angle of 61°. At relatively lower heights (<300 nm for 150 nm pillars with 500 nm spacing), the initial contact angle was less than 80° and the water droplet easily invaded the surface grooves, leading to a reduced contact angle at equilibrium (Wenzel state). At relatively higher heights (>400 nm) on the other hand, the nanostructured PEG surface showed a hydrophobic nature and no significant change in contact angle was observed with time (Cassie–Baxter state). However, due to the hydrophilic nature of PEG, the obtained CAs were relatively low (95°), the contact angle might be further improved by changing the polymer material or optimizing the geometry of the mold.

A similar capillary lithographic approach was demonstrated by Jin *et al.*[81] An alumina membrane was used as the mold for the preparation of aligned polystyrene (PS) nanotubes. The PS solution was cast on glass and the membrane was then brought into contact with the PS cast. After capillary molding, the membrane was dissolved in NaOH and aligned PS nanotubes were obtained. The PS nanotubes showed a contact angle of $162 \pm 1.7°$. The authors concluded that the water droplet was

Table 1 Contact angle of PEG after capillary force lithography[75]

Sample	1	2	3	4
d/nm	150	150	150	150
h/nm	170	310	500	440
h/*d*	1.13	2.07	3.33	2.93
s/nm	500	500	500	500
r	1.3	1.58	1.90	1.79
CA (adv./rec.)	75/46	81/56	95/90	88/81

View Online

Published on 31 January 2007 on http://pubs.rsc.org | doi:10.1039/B602486F
Downloaded on 29 November 2010

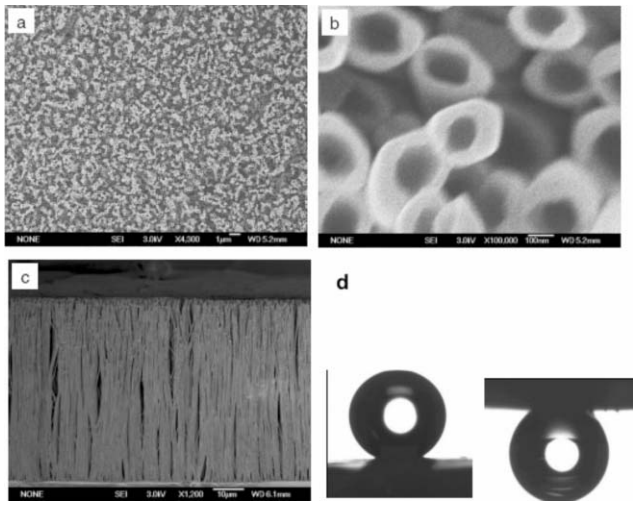

Fig. 9 SEM images of PS nanotubes ((a) top view, (b) magnified image of (a), and (c) side view) and the contact angle behavior (d). (Images reprinted with permission from Jin *et al.*[81] Copyright 2005, John Wiley–VCH.)

in a composite state (the Cassie–Baxter regime). However, it was found that the water droplet does not roll off the surface even at 180° tilt (Fig. 9), indicating that the surface is very sticky, although superhydrophobic. The authors have attributed this super sticky effect to the van der Waals' forces between the water molecules and the high density nanotubes generating a strong adhesion just like the gecko's mechanism.[88] The authors have applied such a sticky surface as a mechanical hand to transfer a water droplet.

Fabrication of superhydrophobic PVA nanofibers were accomplished through extrusion with AAO membranes.[89] The AAO membranes have pores of average diameter of 68.7 nm. Although PVA is a hydrophilic material, the resulting nanofibers showed superhydrophobicity with water contact angle of 171°. The authors attribute this superhydrophobicity to the orientation of the PVA molecules that results in hydrophobic backbones exposed to the surface as confirmed by angle dependent XPS study.

As shown above, templation is a useful technique for the preparation of superhydrophobic surfaces. Depending on the type of templates, many features can be fabricated with tunable surface morphology. Furthermore, templation is versatile in view of the diverse polymeric materials available. The limitations of the templation approaches are that the attainable geometry is limited by the available templates and not every material is suitable for the templation approach.

3.1.2 Photolithography. In photolithographic approaches, light is irradiated through a mask with desired features to the substrates (often silicon) with a photoresist. Subsequent developing and etching steps yield the desired patterned surfaces. Depending on the light source (radiation, electrons), photolithography can be divided into X-ray lithography and e-beam lithography. For the preparation of superhydrophobic surfaces, an extra surface treatment step is needed to render the surfaces hydrophobic. Structures prepared by photolithography are easy to characterize and they are often used for the surface modeling.

Furstner *et al.*[10] created silicon wafers with regular patterns of spikes by X-ray lithography. The wafer was hydrophobicized by sputtering a layer of gold and subsequent immersion in a hexadecanethiol solution. The spikes have a width (d) of 1 or 2 microns, the distance between the spikes (a) were varied from 1 to 5 microns, and the height of the spikes (h) was also varied from 1 to 4 microns. CA of the surfaces varied from 113 to 161° depending on the pillar size, the clearance and the height of the spikes. The self-cleaning property of the specimen was addressed by the application of an artificial fog. A best cleaning surface was found with $d/a = 2$ and $h/d = 4$.

Martines *et al.*[80] have created nanopillars and nanopits on silicon by e-beam lithography (Fig. 10). The center to center pitch is kept constant at 300 nm. The diameter (d) and height (h) of the pillars and pits are varied from sample to sample. The specifications of the samples are shown in Table 2. The hydrophobic nanopatterns were obtained by silanization of the hydrophilic surfaces with octadecyltrichlorosilane (OTS). All surfaces exhibit enhanced hydrophobicity as compared to the flat control surface. For samples with nanopits, the contact angle behavior falls in the Wenzel regime. For samples with pillars, both Wenzel and Cassie–Baxter states were discovered which was ascribed to the differences in aspect ratio (h/d). They disclosed that at given spacing, increasing aspect ratio can dramatically stabilize the Cassie–Baxter regimes as shown by a comparison of the wetting behavior of P22, P21, P13 and P12.

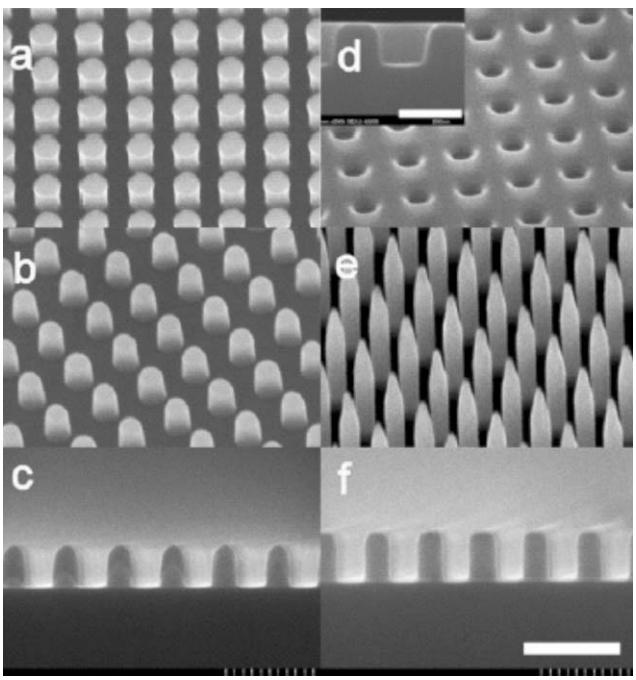

Fig. 10 SEM images of (a) P22 before hydrophobization; (b) P22 after hydrophobization; (c) profile of P22; (d) sample H83 after hydrophobization, the inset shows its profile; (e) P12 after hydrophobization; (f) profile of P21. The profiles were imaged with a 90° tilt, the other images were taken at 45°, scale bar 500 nm (a–f) and 200 nm (inset in (d)), respectively. (Reprinted with permission from Martines *et al.*[80] Copyright 2005, American Chemical Society.)

 This journal is © The Royal Society of Chemistry 2007

View Online

Published on 31 January 2007 on http://pubs.rsc.org | doi:10.1039/B602486F
Downloaded on 29 November 2010

Table 2 Sample specifications and contact angle results of the nanopillars and nanopits[80]

Sample	H90	H83	P22	P21	P13	P12
d/nm	105	138	157	156	124	117
h/nm	116	141	239	239	268	792
l/nm	300	300	300	300	300	300
h/*d*	1.10	1.02	1.52	1.53	2.16	6.77
$\theta_{adv}/\theta_{rec}$	125/92	129/89	155/0	159/140	161/150	164/163

[a] H indicates pits, and P indicates pillars. *d*: diameter of the pits or pillars; *h*: depth or height of feature; *l*: center to center pitch.

3.1.3 Plasma treatment of surfaces. Plasma treatment of surfaces always involves plasma etching. Plasma etching is a dry etch technique in which reactive atoms or ions (such as oxygen, chlorine, fluorine) are generated in a gas discharge. Reactive ion etching makes use of the fact that ions are accelerated in the boundary layer between plasma and substrate with high directivity and are thus able to create deep grooves with steep walls. Plasma treatment of surfaces can cause a considerable change in the surface structure because of the anisotropic etching of the surface layers.

Fresnais *et al.*[44] have used treated low-density polyethylene (LDPE) with plasma etching. Sequential treatment of LDPE with oxygen and CF_4 plasma yielded a surface with CA of 170° and low hysteresis (<5°).[44] The roughness of the resulting surfaces was within the range of 20 to 400 nm.

Minko *et al.*[84] have reported plasma treatment of PTFE for the fabrication of self-adaptive surfaces (Fig. 11). Oxygen plasma etched PTFE showed water CA about 160° without CA hysteresis. The superhydrophobic PTFE surfaces were further treated with ammonia plasma for the incorporation of amino groups in the substrates. These amino modified substrates were then grafted with a mixed polymer brush consisting of two carboxyl terminated incompatible polymers: carboxyl-terminated poly(styrene-*co*-2,3,4,5,6-pentafluorostyrene) (PSF-COOH) and carboxyl-terminated poly(2-vinylpyridine) (PVP-COOH). The grafted surface exhibits switchable wettability upon soaking in different solvents which was ascribed to the enrichment of favored component at the top of the film and the other component collapsing into dimples in the interior of the polymer film (Fig. 12).

There are many more examples using the plasma method for the preparation of superhydrophobic surfaces.[49–51,90–92] As mentioned above, plasma treatment is a dry etching technique, thus rough surfaces are easily obtained after the plasma treatment. Furthermore, depending on the type of gas, tetrafluomethane, ammonia, argon or oxygen, different elements can be easily introduced in the surface, providing additional functions.

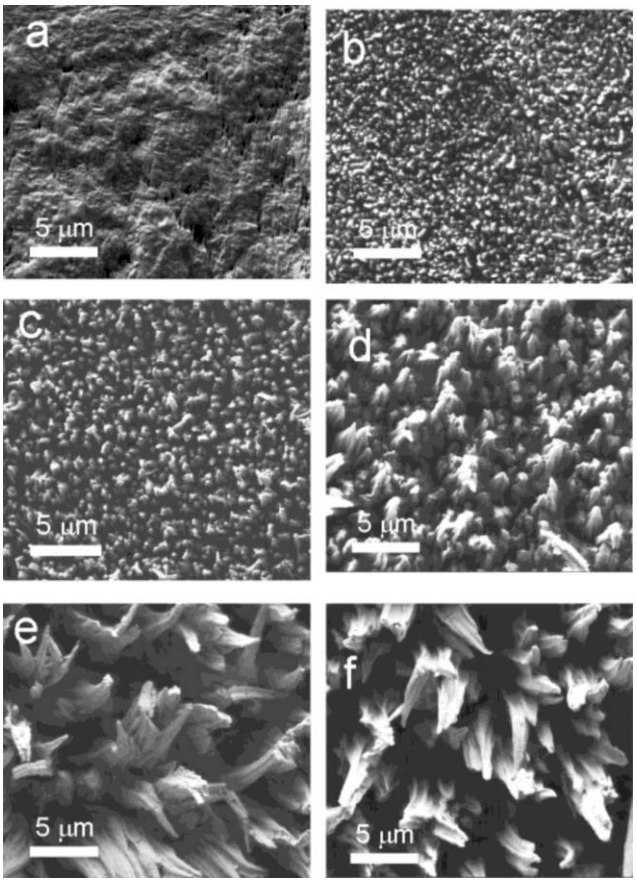

Fig. 11 Scanning electron micrographs of PTFE foils: untreated (a); treated with oxygen plasma for 60 s (b), 120 s (c), 5 min (d) or 10 min (e); and treated with oxygen plasma for 10 min + NH_3 for 1 min (f). (Reprinted with permission from Minko *et al.*[84] Copyright 2003, American Chemical Society.)

3.2 Bottom up approaches

Contrary to the top-down approach, bottom-up methods involve the building (or designing) larger, more complex objects by integration of smaller building blocks or components. The bottom-up approach in nanofabrication involves often self-assembly and self-organization. Self-assembly is an integration method where components spontaneously

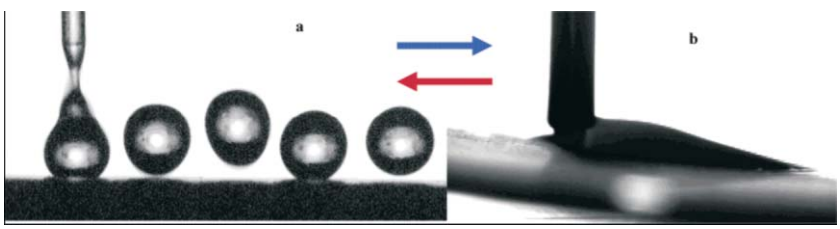

Fig. 12 Photograph of a water drop deposited onto the self-adaptive surface: the image shows that a water drop jumps and rolls on the ultrahydrophobic surface obtained after exposure of the sample to toluene (a). In contrast, exposure to acidic water switches the sample to a hydrophilic state and the water drop spreads on the substrate. (Reprinted with permission from Minko *et al.*[84] Copyright 2003, American Chemical Society.)

View Online

Published on 31 January 2007 on http://pubs.rsc.org | doi:10.1039/B602486F
Downloaded on 29 November 2010

assemble in solution or the gas phase until a stable structure of minimum energy is reached. Bottom-up approaches that have been applied for the preparation of superhydrophobic surfaces include chemical deposition methods such as chemical bath deposition (CBD),[51,63,64,66] chemical vapor deposition (CVD),[63,64] and electrochemical deposition,[60,62,65] layer-by-layer (LBL) deposition *via* electrostatic assembly,[52,57] colloidal assembly,[59,68,70] sol–gel methods,[35,57,70,93–104] hydrogen bonding,[67] and chemical synthesis.[105] In the following paragraphs, some important examples will be given and discussed in detail.

3.2.1 Chemical deposition. Chemical deposition takes place in a chemical reaction, where the product self-assembles and deposits on a suitable substrate. Chemical deposition is commonly used for generating thin films of crystalline inorganic materials, such as ZnS, CuSe, InS, CdS *etc.* Depending on the deposition conditions, several terms have been used such as chemical bath deposition (CBD), chemical vapor deposition (CVD), and electrochemical deposition. Depending on the material and the deposition conditions, different surface morphologies have been obtained from nanopins, nanotubes to nanorods.

Hosono *et al.*[106] have used CBD for the creation a of nanopin film from a solution of $CoCl_2$ and NH_2CO in water. The film was deposited on commercial borosilicate glass slides in an autoclave. Because each metal complex in the solution is singly deposited on the surface based on thermodymanic equilibrium conditions, single crystalline-like structures are formed. After deposition, the nanopin was modified with lauric acid (with θ = 75.1). A picture of the nanopin is shown in Fig. 13. The top of the needle is very sharp with a diameter of 6.5 nm. The water CA of the resulted film is 178°, which is the highest contact angle that has been reported so far.

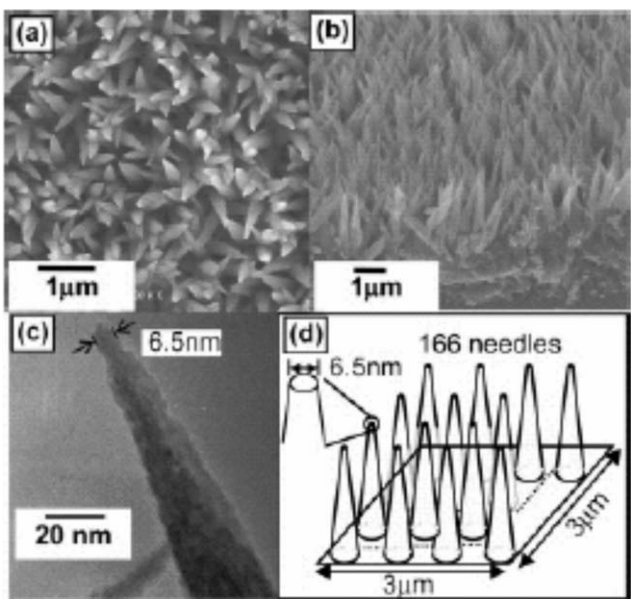

Fig. 13 (a, b) Field emission SEM images of the cobalt hydroxide films observed from the top and side, respectively. (c) TEM images of the cobalt hydroxide films. (d) A simple model of the film with the fractal structure. (Reprinted with permission from Hosono *et al.*[106] Copyright 2005, American Chemical Society.)

Wu *et al.*[107] also used CBD for the preparation of superhydrophobic surfaces of zinc oxide (ZnO) nanorods on glass slides starting from a solution mixture of $Zn(NO_3)_2$, NH_4Cl, urea, and ammonia. ZnO nanorods with diameters ranging from 400 to 600 nm form a uniform and dense film on the substrates. The surfaces were then modified with SAMs of alkanoic acids of different chain length. All the SAM modified surfaces showed high advancing contact angle (>150°), the receding angles of the surfaces depends strongly on the chain length of the alkanoic acids.

Huang *et al.*[108] have prepared aligned carbon nanotubes by chemical vapor deposition on a Fe–N coated silicon substrates. After the deposition a ZnO layer, the substrates showed water CA of 159°. The surface, however, became hydrophilic after prolonged exposure to UV illumination. The hydrophobicity of the surface can be restored after storage in the darkness. This tunable wettability is interesting in microfluidic devices.

Other chemical deposition methods such as electrochemical deposition of the zinc oxide,[65] gold clusters,[109] or silver aggregates have been used to prepare superhydrophobic surfaces.[60] In these examples, the deposited structures were modified with SAMs to render hydrophobicity.

3.2.2 Colloidal assemblies. Monodispersed particles can form close packed assemblies on surfaces because of van der Waals interactions. The particle assemblies render roughness to the underlying substrates. Further treatment such as plasma etching[110] can also be applied to improve the roughness. The colloidal particles can vary from polymer beads to inorganic spheres. Colloidal assembly is cost effective since no expensive lithographic technique is required. This method is easy to master and to apply under laboratory conditions.

Monodipersed polystyrene (PS) beads can form closely packed superhydrophobic surfaces by spin coating.[110] Oxygen plasma etching was used to control the solid–air fraction of these nanostructures. The sizes of beads were reduced by controlling the etching conditions. After plasma treatment, the surfaces were coated with a layer of gold and eventually a layer of octadecanethiol SAM to render hydrophobicity. SEM images of the PS beads and the corresponding water CA are shown in Fig. 14.

Zhang *et al.*[59] have used binary colloidal assemblies for the creation of superhydrophobic surfaces. $CaCO_3$-loaded hydrogel spheres were dip-coated on silicon substrates (Fig. 15). These assemblies were employed as templates for the self-assembly of silica nanoparticles or polystyrene beads. Due to the hydrophilicity difference between silicon wafers and $CaCO_3$-loaded hydrogel spheres, the regio- selective localization of silica or polystyrene spheres leads to irregular binary structures with a hierarchical roughness. The subsequent modification with deposition of gold and SAM formation yield superhydrophobic surfaces with water CA of 160° for silica based assembly and 156° for PS based assembly.

3.2.3 Layer-by-layer deposition. Layer-by-layer (LBL) deposition takes advantages of the electrostatic charge interactions between the different layers such as polyanion and polycation. The LBL technique is easy to perform and allows controlling the thickness of the resulting layer with

 This journal is © The Royal Society of Chemistry 2007

View Online

Published on 31 January 2007 on http://pubs.rsc.org | doi:10.1039/B602486F
Downloaded on 29 November 2010

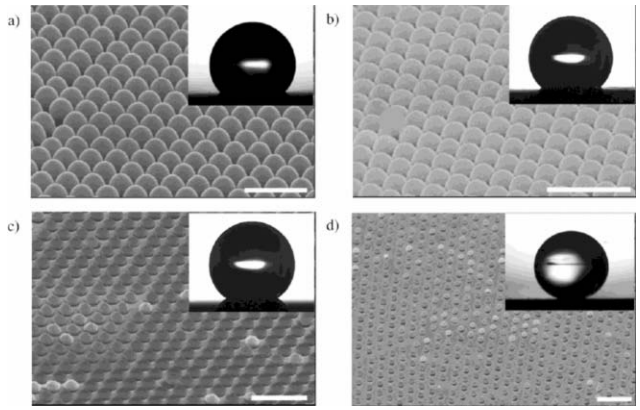

Fig. 14 SEM images (60°) of the size-reduced polystyrene beads and the water contact angle measurement on the corresponding modified surfaces (insets). The diameters of polystyrene beads and water contact angles on these surfaces were measured to be (a) 400 nm, 135°, (b) 360 nm, 144°, (c) 330 nm, 152° and (d) 190 nm, 168°. Bar: 1 μm. (Reprinted with permission from ref. 110. Copyright 2004, American Chemical Society.)

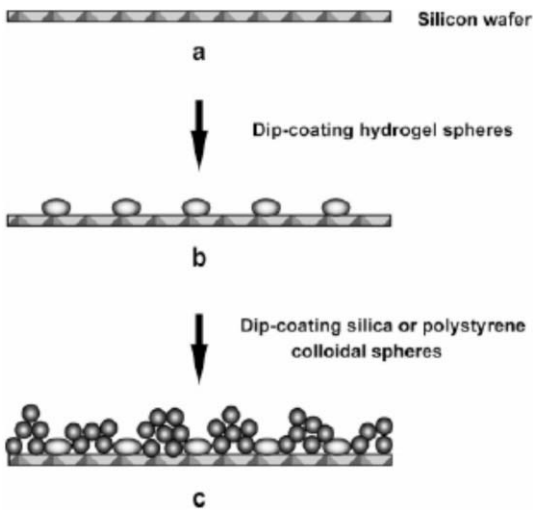

Fig. 15 Schematic illustration of the binary assembly procedure on silicon wafers by consecutively dip-coating $CaCO_3$-hydrogel particles and silica or PS colloidal spheres. (Reprinted with permission from Zhang *et al.*[59] Copyright 2005, American Chemical Society.)

molecular precision. Polyelectrolytes are hydrophilic, therefore, a hydrophobizisation is always necessary. Nanoparticles are often incorporated into the multilayer system in order to enhance the roughness effects. However, the multilayer films can also be roughened by some additional treatment. Zhai *et al.*[111] have prepared superhydrophobic silicon surfaces using polyallylamine hydrochloride (PAH)/poly(acrylic acid) (PAA) multilayers *via* LBL deposition. By using an appropriate combination of acidic treatments, pores on the order of 10 microns and a honeycomb-like structure were formed on the PAH/PAA films (Fig. 16(A) and (B)). The honeycomb-like polyelectrolyte multilayer surface was further coated with silica nanoparticles (Fig. 16(C)). Superhydrophobicity was achieved by coating this highly textured multilayer surface with a semifluorinated silane. The stability of the surface was

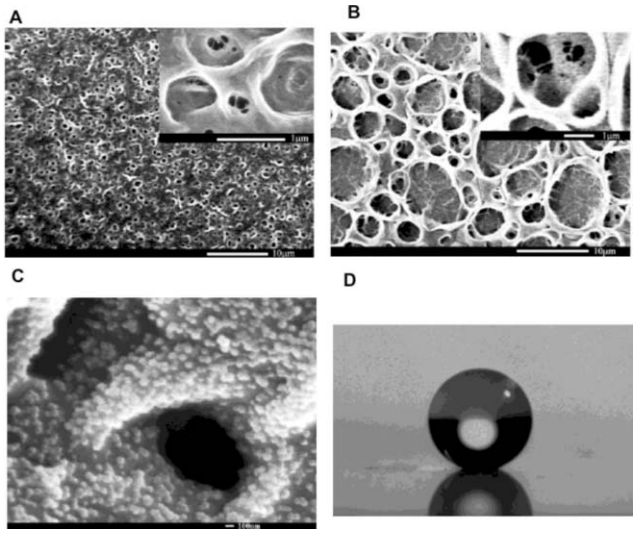

Fig. 16 SEM images of $(PAH/PAA)_{100.5}$ films after a single acid treatment (A) and after a combined acid treatment (B). (C) SEM image of the fully treated structure (B) with silica nanoparticles. (D) Water droplet on this superhydrophobic surface. (Reprinted with permission from Zhai *et al.*[111] Copyright 2004, American Chemical Society.)

tested by extended immersion in water. It was found that both the microstructure created by the combined acid treatments and the nanostructure induced by the deposition of silica nanoparticles are necessary to create stable superhydrophobic surfaces.

Based on Zhai's work, Jisr *et al.* have further developed a simplified method for the preparation of superhydrophobic surfaces using polyelectrolytes.[112] The molecular structures of the polyelectrolytes are shown in Scheme 1. The polyanions and polycations are fluorinated polyelectrolytes, Nafion and fluorinate poly(vinylpyridine) (PFPVP), and "normal" PDADMA and PSS. For the fluorinated polyelectrolytes, no extra hydrophobic coating was necessary. The flat multilayer showed a static contact angle of 114° with 10 double layers. Incorporation of clay mineral attapulgite (naturally occurring

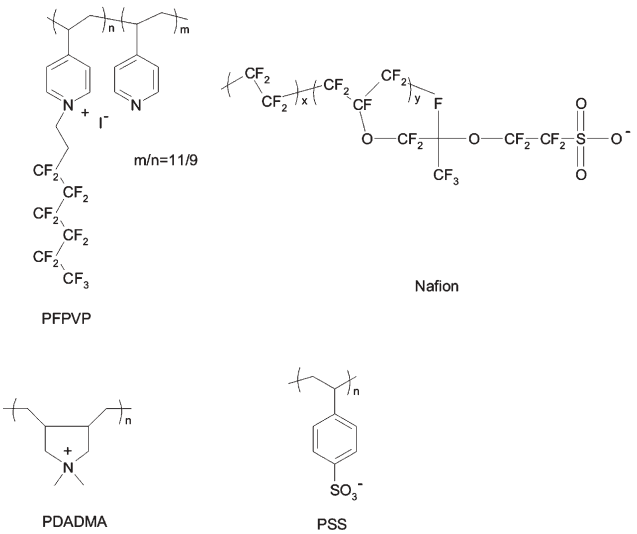

Scheme 1

View Online

Published on 31 January 2007 on http://pubs.rsc.org | doi:10.1039/B602486F
Downloaded on 29 November 2010

nanorods) into the multilayers produced ultraphobic surfaces (CA 168°) with a sliding angle less than 1°.

Han *et al.*[52] have demonstrated another approach for the incorporation of particles in the LBL assembly for the preparation of superhydrophobic surfaces. PAA coated ZrO_2 particles were deposited alternately with PAH (polyallyamine hydrochloride) on clean silicon substrates. After 20 deposition cycles, the surface showed water contact angle of 139° for a PAH exposed outermost layer with a huge hysteresis ($\pm$40°). These results are noteworthy since PAH is rather hydrophilic ($\pm$60°). Further deposition of silica nanoparticles and dipping the film in the solution of perfluorinated dodecyltrichlorosilane decreased the contact angle hysteresis and improved the superhydrophobicity significantly. The substrates showed a water contact angle of 170° with a hysteresis of 2°. Amidation by thermal treatment of substrates at an elevated temperature of 220 °C was utilized to render the film extra stability.

The LBL technique is easy to perform and allows molecularly precise control of the film thickness. However, polyelectrolytes are hydrophilic, therefore, a hydrophobizisation is often necessary. In addition, to generate rough surfaces, some additional steps are needed such as the incorporation of nanoparticles, thus making it less straight forward for the preparation of superhydrophobic surfaces.

3.2.3 Sol–gel methods. A sol is usually prepared by hydrolysis of the corresponding oxide in the presence of solvent. During the network formation process, a large amount of solvent are also impregnated in the network and thus a gel is formed. Silica sols are normally prepared by hydrolysis and condensation of orthosilicate. The sol can be applied either directly or combined with fillers such as silica nanoparticles. The resulting surface property depends on how the sol was prepared and surface functional groups of the resulted gel.[35,57,70,93–104]

Shang *et al.*[113] have prepared optically transparent superhydrophobic silica-based films by means of sol–gel processing and self-assembly. Desired surface roughness was obtained by tuning the microstructures of the sol–gels through careful control of hydrolysis and condensation reactions of various silica precursors during sol–gel processing, whereas modification of surface chemistry was done by introducing a monolayer through surface condensation reaction. Such coatings were obtained by dip-coating the silica sols directly onto substrates. The resulting silica-based coatings showed optical transparency higher than 90% and a reflection lower than 10%. The best advancing and receding water contact angles were approximately 165 and 115°, respectively, indicating a relatively large contact angle hysteresis. The authors did not provide any solution to solve this problem.

Hikita *et al.*[35] have used the sol–gel method for the preparation of super liquid repellent surfaces. Both surface energy and roughness were controlled using colloidal silica particles and fluoroalkylsilane. For films with optimal ratio between colloidal silica and fluoroalkylsilane, the surfaces exhibited repellency to both water and oil. This method provides a simple one-pot coating for a large area.

Doshi *et al.*[114] used silica sol–gel for the creation of surfaces with tunable properties from superhydrophobic to superhydrophilic. A low-temperature, low-pressure technique was used to prepare a rough and highly porous organosilica aerogel-like film (Fig. 17). The superhydrophobic coatings were made from a precursor solution containing mixed alkoxides 3,3,3-trifluoropropyltrimethoxysilane (TFPTMOS) and tetramethylorthosilicate (TMOS). A film thickness of 50 nm was obtained. CA consistently reached 155–160°, and angles up to 170° have been observed. UV/ozone treatments were used to control the surface coverage of hydrophobic organic ligands on the silica framework, allowing the CA to be continuously varied over the range of 160° (superhydrophobic, with presence of organic ligands) to <10° (hydrophilic, after removal of the organic ligands).

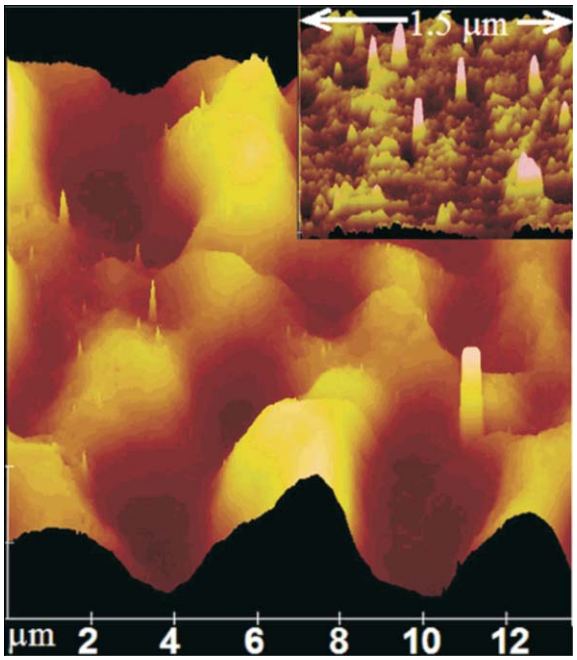

Fig. 17 AFM image of SH film in air measured over an area of 13.5 μm × 13.5 μm. The inset shows another image at a higher magnification measured over an area of 1.5 μm × 1.5 μm. (Reprinted with permission from Doshi *et al.*[114] Copyright 2005, American Chemical Society.)

The advantages of the bottom-up approach are the molecular control of the chemistry, composition, even the thickness of the products. Nevertheless, it is difficult to predict the hydrophobic properties until the last step.

3.3 Combination of bottom-up and top-down approaches

The combination of bottom-up and top-down approaches might have the apparent advantages of both techniques. It is especially useful for the creation of architectures with a two-scale roughness, resembling the structure of the lotus leaf. The combination methods often consist of two stages. Typically, the first step is the top-down approach for the creation of a rough surface and the second step is bottom-up process for the creation of the fine roughness. However, some combination methods do not necessarily show a distinct two-stage process. For example, phase separation involves casting of thin film and subsequent phase separation by controlling the environmental conditions.

 This journal is © The Royal Society of Chemistry 2007

View Online

Published on 31 January 2007 on http://pubs.rsc.org | doi:10.1039/B602486F
Downloaded on 29 November 2010

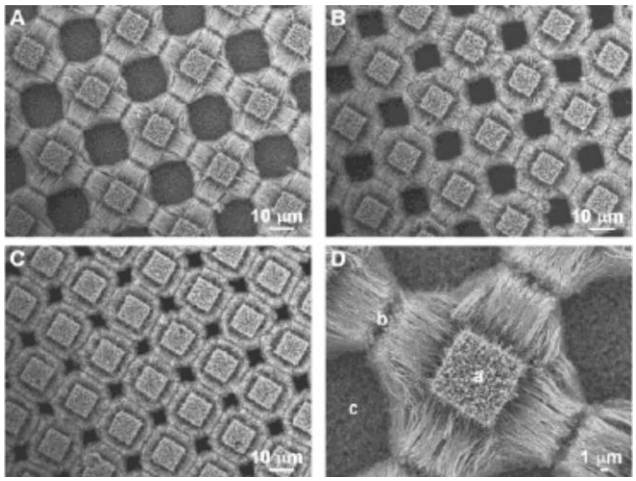

Fig. 18 SEM images of three-dimensional anisotropic ACNT microstructures constructed by the CVD method on silicon substrates with a well defined quadrate micropillar array. (A, B and C) Periodic ACNT arrays with pillar spacings of 20, 15 and 10 μm, respectively. (D) Magnified image of mutually orthogonal ACNT arrays on a single silicon pillar of image (A); (a) vertical ACNT array on the top face of a pillar; (b) horizontal ACNT array grown from the side faces of the pillar; and (c) ACNTs grown from the bottom between the pillar arrays. (Reprinted with permission from Sun *et al.*[115] Copyright 2003, American Chemical Society.)

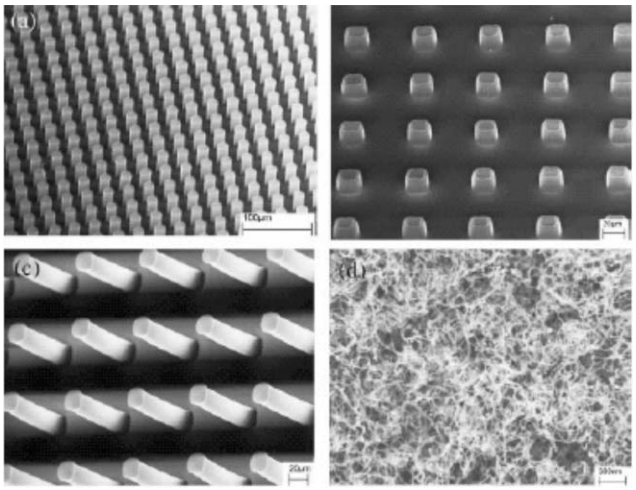

Fig. 19 Typical SEM images of CNT arrays on silicon substrates: (a) cylindrical CNT arrays with 6 μm radius, 30 μm pitch, and 25 μm height; (b) cylinder CNT arrays with 10 μm radius, 60 μm pitch, and 11 μm height; (c) cylindrical CNTs arrays with 10 μm radius, 60 μm pitch, and 90 μm height; (d) as-grown CNT array surfaces. (Reprinted with permission from Zhu *et al.*[116] Copyright 2005, American Chemical Society.)

3.3.1 Combination methods based on chemical vapor deposition (CVD). Sun *et al.*[115] have demonstrated the preparation of superhydrophobic anisotropic aligned carbon nanotubes (ACNT) film by chemical vapor deposition (CVD) on silicon substrates with quadrate micropillar arrays prepared by photolithography. The carbon nanotubes packed densely and were quite uniform in length at about 10 microns as shown in Fig. 18. Both hydrophobic and hydrophilic surfaces were observed depending on the spacing between the pillar arrays, which was ascribed to the anisotropic nature of the carbon nanotube arrays. However, when the film was coated with a fluorinated SAM of (2-(perfluorooctyl)ethyl)trimethoxysilane, all surfaces are superhydrophobic and the spacing effects were not observed.

In a similar approach Zhu *et al.*[116] also prepared surfaces with two-scale roughness by controlled growth of carbon nanotube (CNT) arrays by CVD (Fig. 19). To compare wetting on micropatterned silicon surfaces with wetting on nanoscale roughness surfaces, two model systems were fabricated: carbon nanotube arrays on silicon wafers and carbon nanotube arrays on carbon nanotube films. In the latter case, the CNT array size, pitch, and height have been varied to explore geometric effects on surface hydrophobicity. Compared to patterned Si surfaces with similar geometrical sizes, the nanoscale roughness does not significantly increase the apparent water contact angle. Thus, the microscale roughness determines the apparent water contact. However, the introduction of nanoscale roughness can decrease the contact angle hysteresis to less than 1° and improve the stability of the superhydrophobic surfaces.

3.3.2 Combination methods based on membrane casting. Membrane casting is normally used for the preparation of porous structures. Most polymer membranes are prepared by casting a polymer solution *via* a suitable template, where microscopic structures are formed through phase separation. Phase separation occurs when a polymer solution close to the cloud point is submerged in nonsolvents or subjected to heat treatments. Because of the interaction of solvent and nonsolvents with the macromolecules, the polymer nucleates resulting in polymer rich and polymer poor phases. At the polymer rich phase, the macromolecules nucleate and form the networks. In the polymer poor phase, after the solvent removal, pores are formed.[117]

Erbil *et al.*[118] have used isotactic polypropylene (i-PP) for the preparation of superhydrophobic surfaces by controlling the selection of solvents and temperature. Xylene was used as solvent of the polymer and different nonsolvents were tested. A series of samples were tested at different solute concentration, drying temperature, and different nanosolvents. It was found that lowering the drying temperature facilitates a loose network formation (Fig. 20). Methyl ethyl ketone was found to be the best nonsolvent and resulted in a surface with contact angle of 160°.

Following Erbil's work, Lu *et al.*[119] used low density polyethylene for the preparation of superhydrophobic surfaces by thermally induced phase separation. By changing the duration of heat treatment, they have been able to control the structure of the eventual film and finally the wettability of the surfaces.

Xie *et al.*[120] have prepared super-amphiphobic polymeric coatings with a single casting process with two polymer materials: poly(methyl methacrylate) (PMMA) and fluorine-end-capped polyurethane (FPU). For films containing only PMMA, water CA of 145° was found. SEM studies showed rough structures with micropapillae (Fig. 21(b)). For the mixture of PMMA and FPU, films posses both micro- and nanopapillae with water CA of 166°. The lotus like

View Online

Published on 31 January 2007 on http://pubs.rsc.org | doi:10.1039/B602486F
Downloaded on 29 November 2010

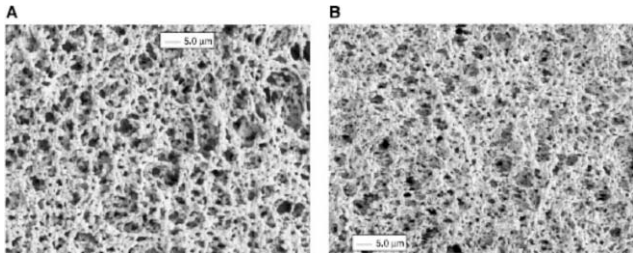

Fig. 20 SEM pictures of i-PP obtained from a solution (20 mg ml^{-1}) in *p*-xylene on glass slides at drying temperatures of (A) 30 °C and (B) 60 °C. The i-PP was dissolved in *p*-xylene at 130 °C and the solvent was evaporated in a vacuum oven at the specified temperatures. The surfaces of the i-PP coatings were sputter-coated with 1-nm thick gold before the measurements were taken. The measurements were taken at 1 keV. The magnification is 1000×. (Images adapted from Erbil *et al.*[118] with permission.)

micro–nano binary structure and low surface energy of the FPU was ascribed to the high CA and low sliding angle of the surface.

Yabu and Shimonura[121] have used block copolymers containing equimolar fluorinated acrylate and methylmethacrylate monomers for the preparation of superhydrophobic surfaces. The polymer solution was cast on a substrate by a blade. Careful controlling the condensation of water droplets and final evaporation of the solvent and water yielded a

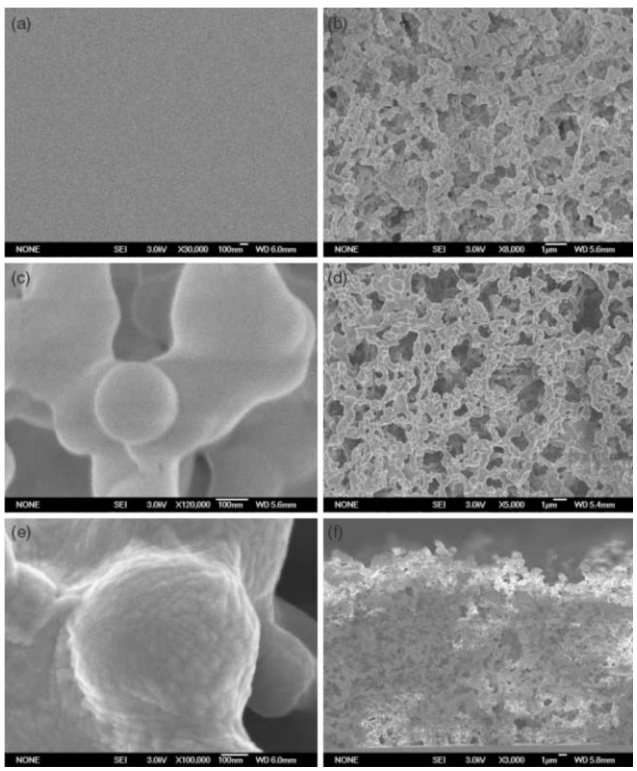

Fig. 21 SEM images of FPU/PMMA mixtures: (a) pure FPU film; (b) film of pure PMMA; (c) enlarged image of (b); (d) mixture of PMMA/FPU; (e) enlarged image of (d); (f) cross sectional view of the mixture surface. (Images reprinted with permission from Xie *et al.*[120] Copyright 2004, Wiley–VCH.)

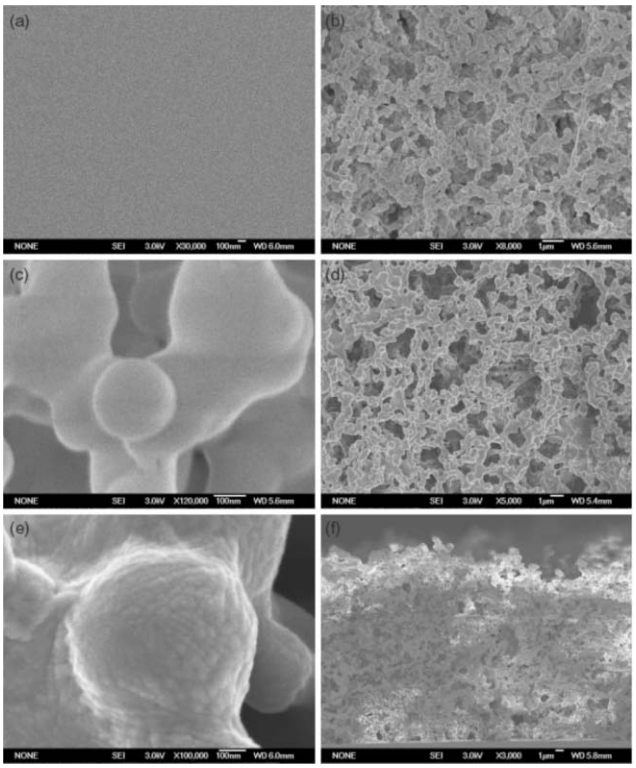

Fig. 22 Schematic illustration and scanning electron micrograph of (a) the honeycomb-patterned film, (b) the peeling process, and (c) the pincushion structure. (Reprinted with permission from Yabu and Shimonura.[121] Copyright 2005, American Chemical Society.)

honeycomb film (Fig. 22). The pore size over the major part of the film was 300 nm. Pin cushion structures were obtained after peeling off the upper layer of the honeycomb film. The sizes of the honeycomb and pincushion structures were easily controlled by varying the casting volume of polymer solution. A superhydrophobic surface with the maximum contact angle of 170° was observed for pincushion structures prepared from honeycomb films with 1.6 μm pores.

Recently, Wessling's group has reported superhydrophobic surfaces with two-scale roughness prepared in a single step by casting of membrane solution of Hyflon AD.[122] This process is denoted as phase separation micromolding (PSμM). The films were prepared by casting Hyflon AD solution on a silicon template patterned by photolithography. The patterns on the templates were optimized separately. This method provides a surface that contains roughness on two independently controllable levels, *i.e.*, the microstructure level (from the template) and the level of porosity stemming from the phase inversion (Fig. 23).

In conclusion, membrane casting is relatively easy to perform because the roughness is generated during the film formation process. However, in order to get optimized results, many parameters have to be adjusted such as the selection of solvents, nonsolvents, the solution concentration, and the conditions for membrane casting. Nevertheless, the phase separation micromolding[122] appears to be a promising technique in the preparation of superhydrophobic surfaces.

 This journal is © The Royal Society of Chemistry 2007

View Online

Published on 31 January 2007 on http://pubs.rsc.org | doi:10.1039/B602486F
Downloaded on 29 November 2010

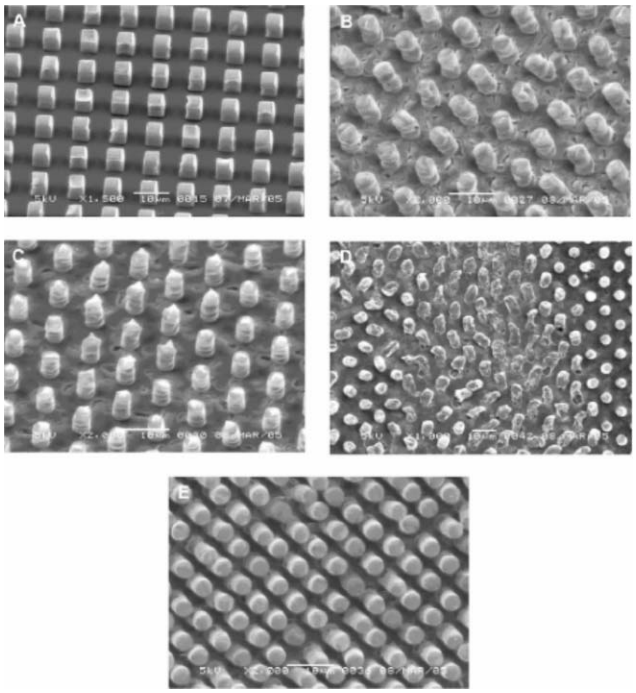

Fig. 23 Surfaces prepared from Hyflon AD by PSμM.[122] (A) a Hyflon AD H80 structure of square pillars prepared by evaporating a Hyflon AD H80 solution on a mold; (B and C) Hyflon AD H80 microstructures of pillars; (D) a surface of Hyflon AD H60; (E) the protrusions of a microstructure of closely packed pillars with limited superimposed roughness. (Reprinted with permission from Vogelaar *et al.*[122] Copyright 2006, American Chemical Society.)

3.3.3 Micelles. Surfactants in solution are often association colloids, that is, they tend to form aggregates of colloidal dimensions, which exist in equilibrium with the molecules or ions from which they are formed. Such aggregates are termed micelles. Similar to phase separation, micelles are formed due to the microscale phase separation. Block copolymers usually form micelles when dispersed in a selective solvent as a result of the different solubility of the blocks.[123,124] The cast block polymer micelles when exposed to humid environments will form films of different morphology depending on the relative humidity.

Micelle solutions of PS-*b*-PDMS block copolymer were used for the preparation of superhydrophobic surface by vapor induced phase separation.[123] Depending on the solvents used, and humidity of the air, surfaces with different wetting behaviors were observed. For superhydrophobic surfaces, enrichment of PDMS block in the outermost surface was observed with CA of 163° (Fig. 24), which was attributed to the rearranging of PDMS block to the surface during the phase separation process.

Han *et al.*[125] used block copolymer of PtBA-*b*-PDMS-*b*-ptBA micelle solution for the preparation of superhydrophobic surfaces which gave surfaces with water contact angle up to 163°. In a second approach, silica nanoparticles were incorporated into the micelle solution. The surface has a contact angle of 170°, the sliding angle is less than 2°.

Similar to membrane casting, superhydrophobic films based on micelles depend on the selection of solvents and the block

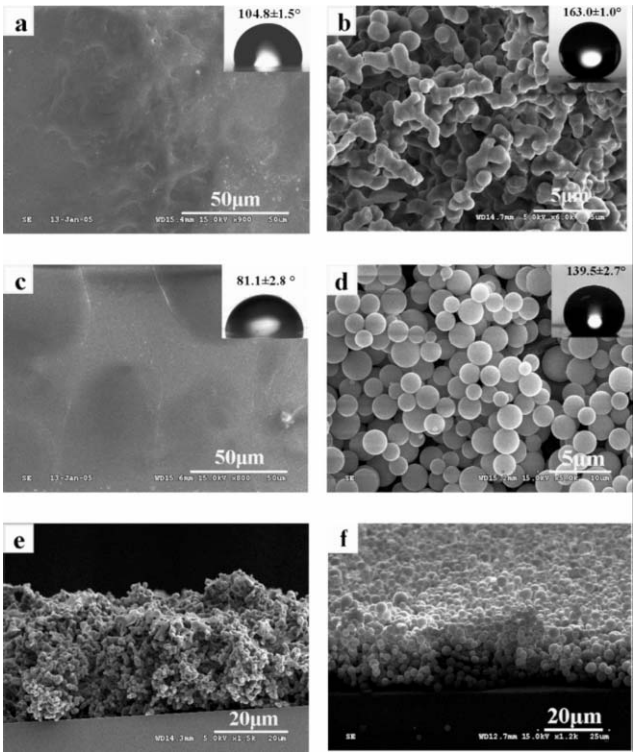

Fig. 24 SEM images of the surfaces cast from a 5 mg mL^{-1} micellar solution of PS-*b*-PDMS in DMF in the (a) dry and (b) humid air and from 5 mg ml^{-1} homopolymer solution of PS in DMF in the (c) dry and (d) humid air at room temperature, respectively. The relative humidity of the dry atmosphere is less than 10% while for the humid air is 60.5%. (e) and (f) are the side view of (b) and (d), respectively. Insets are the water CA of each surface. (Reprinted with permission from Zhao *et al.*[123] Copyright 2005, American Chemical Society.)

copolymers. The morphologies of the obtained films are dependent on the casting methods, relative humidity of the environment *etc*. Because of the availability of a diversity of polymer materials, superhydrophobic surfaces with diverse structures have been reported.[124,125]

3.3.3 Electrospinning. Electrospinning is normally used for the preparation of polymer nanofibers. It is an extrusion process where an electrical bias is applied from the extrusion nozzle and a grounded collection plate.[126] Electrospun films consist of a continuous, nonwoven web of fibers. Along the trajectory of the extruded polymer fiber most of the solvents evaporate such that a thin film is formed. In addition to surface roughness, the film properties can be optimized by chemical modification, such as the introduction of fluorine.[74]

Electrospinning has been applied for the fabrication of superhydrophobic films of polymers alone[74,127] or in combination with other methods, such as chemical vapor deposition.[63] The topography of the electrospun film can be tuned from predominantly beads to only fibers by increasing the viscosity of the polymer solution as shown by Acatay *et al.*[74] The morphology was found to play an important role in the final wetting behavior. Surfaces with beads are more hydrophobic than those containing only nanofibers. Based on these observations, lower molecular weight polymers were used

View Online

Published on 31 January 2007 on http://pubs.rsc.org | doi:10.1039/B602486F
Downloaded on 29 November 2010

giving even higher water contact angles because low molecular polymer yielded more bead formation than the high weight molecular polymers. The highest static contact angle of the films made of low molecular weight polymers was around 167°.

Ma *et al.*[63] showed the combination of electrospinning of poly(caprolectone) (PCL) with initiated chemical vapor deposition (i-CVD) of polymerized perfluoroalkyl ethyl methacrylate (PPFEMA). The hierarchical surface roughness inherent to the PCL electrospun films and the extremely low surface free energy of the coating layer obtained by i-CVD yields stable superhydrophobicity with a contact angle of 175° and a threshold sliding angle less than 2.5° for a 20 mg water droplet. Because of the low surface energy coating PPFEMA, the resulting surfaces not only showed high hydrophobicity (water CA up to 175°) but also high oleophobocity (118° for decane).

4 Modeling the superhydrophobic surfaces

As stated in section 2, both Wenzel and Cassie–Baxter theories give only a qualitative prediction of roughness effects. In practice, the conclusion comes always after the wettability measurements. It is critical in designing superhydrophobic substrates to predict accurately the wetting state. Moreover, often the question arises as whether there is an optimal surface geometry for wetting. This problem has been addressed by many groups. The results have been controversial so far. In the following paragraph, we will summarize the controversy and try to give an unbiased opinion on the results.

4.1 The roughness factor

According to Wenzel's theory, the roughness factor plays an important role in determining the wettability of the surface where the roughness effects enhance both the hydrophocity and the contact angle hysteresis. However, in the Cassie–Baxter theory, no roughness effect is considered.

Regularly textured surfaces are often used for modeling the surface wetting behavior because the shape, height, and surface coverage are easily monitored and many parameters can be easily calculated. Bico *et al.*[128] were among the pioneers in modeling regularly textured superhydrophobic surfaces with spikes, holes, and stripes. Substrates with specified roughness were prepared *via* templation and sintering of silica gel. The surfaces were functionalized with silane SAMs to render them hydrophobic. Regardless of the value of the roughness factor of the resulting surfaces, all surfaces showed contact angles that meet the CB prediction. Accordingly, it was concluded that for hydrophobic surfaces, the apparent contact angle is a sole function of solid fraction or air fraction. However, it must be pointed out that for the surfaces with holes, the static contact angle is 131° with a huge hysteresis (63°). In this sense, it is hard to conclude that the water droplet on the substrate is in a composite state as the authors have indicated and that the large hysteresis was due to the water retained in the holes at the retraction.

Patankar[79] has modeled surfaces with square posts. The modeling was based on minimized energy during the drop forming process. Contrary to Bico's conclusion, his results recommend to use high pillars at given pillar size (high roughness factor). Further periodic spacing between the pillars renders the substrate insensitive to whether a wetted contact or a composite contact is formed. The model was tested with the data of Bico *et al.*,[128] which showed very good agreements.

Lundgren *et al.*[129] have reported molecular dynamics modeling of the different wetting properties of the top and the sides of the pillars, which play an important role in determining the contact angle. For low pillar heights (h), the system is in the Wenzel regime and a change to the Cassie–Baxter regime is seen when the pillar height was increased. The contact angles seem to be independent of the pillar height when h exceeds 15 Å.

Extrand[130] has developed a linear model for predicting contact angle and hysteresis on rough and ultraphobic surfaces. In his model, a linear relationship between the apparent contact angle and the Young' contact angle was used to predict the dynamic contact angles by taking into consideration the contact line fraction of the asperities instead of the solid fraction, which is a modified expression of Cassie–Baxter's equation. Extrand compared his theoretical calculation of Oner and McCarthy's[33] designs with the theoretical predictions of the Wenzel and Cassie–Baxter models. The comparison showed that the advancing contact angles and contact angle hysteresis fit Extrand's prediction very well. For determining the state of wetting, a parameter was introduced denoted as contact line density. This parameter is determined by the length of asperity perimeter per unit area that could potentially suspend a water droplet. The criteria for suspension or penetration were established by a critical contact line density, which was determined by examining the balance between the body weight of the drop and the surfaces forces. When the textures have contact line density values higher than the critical value, drops will suspend, otherwise, the drop will collapse. These criteria are quite useful in predicting how the designed surfaces will behave. It is also interesting, here, that again the superhydrophobic state is not related to the etch depth of the posts as predicted in Cassie–Baxter's theory. Using Bico's data, Extrand also showed the models's ability to correctly predict experimental observations. In conclusion, the author suggested that for the superhydrophobic state, a sole roughness or solid fraction is insufficient, other factors such as asperity slopes, liquid density, and surface tension must be considered.

The Extrand models predict the contact angle variations. Since the model has been tested with many research data, it has proven to be very versatile in predicting contact angles and contact angle hysteresis. However, this model does not address the observed transitions from suspensions to collapsed drops.

4.2 Transition state

It has been observed that a water drop on a superhydrophobic surface can transit from a composite to a fully wetted state.[76,128] Water drops on these type of surfaces are in a metastable state and upon external disturbance transitions from one state to another are evident. He *et al.*[76] have shown that depending on how the drop is placed, both suspension and wetting state were observed. Even a lotus leaf can be wetted depending on how the water drops were formed.[131]

 This journal is © The Royal Society of Chemistry 2007

View Online

Published on 31 January 2007 on http://pubs.rsc.org | doi:10.1039/B602486F
Downloaded on 29 November 2010

Nosonnovsky and Bhushan[132] have used a stochastic model to simulate the metastable state. For a rough surface, increased solid–liquid interfacial area results in increased interface energy and higher contact angle for non-wetting liquids. For a very rough surface, a composite solid–liquid–air interface may form air pockets trapped in the valleys between asperities, as opposed to the homogeneous solid–liquid interface. Both the fully wetted and composite interface configurations correspond to local energy minima of the system and therefore, there are stable states associated with different energy levels. The system may transform from one stable state to the other due to small perturbations, such as capillary waves. Based on this model, the authors propose that distances between the asperities should be long. The energy theory also agrees with others, however, the authors did not use any available data to fit their model.

Patankar[78] explained the metastable state also in terms of the energy argument. The two distinct contact angles are stable equilibrium positions, *i.e.* they are all local minimum energy states, but one has a lower energy level than the other. The lower contact angle has a global minimum energy. To move one equilibrium position to the other, an energy barrier has to be overcome, such as that squeezing the water droplet changes the apparent contact angle reported by Bico *et al.*[128]

Zheng *et al.*[133] have modelled thoroughly the underlying mechanisms of stability, metastability, or instability of the Cassie–Baxter and Wenzel wetting modes and their transitions on superhydrophobic surfaces decorated with periodic micro-pillars quantitatively. A pillar slenderness ratio η was introduced and defined a function of the pillar height (H), perimeter (L), and area (A).

$$\lambda = \frac{A}{L} \qquad \eta = \frac{H}{\lambda} = \frac{HL}{A} \tag{5}$$

η_e (*i.e.*, the equienergy slenderness ratio) was derived by energy analysis and is formulated as a function solid fraction (f) and Young's contact angle (θ) as follows:

$$\eta_e = -\frac{1-f}{f}\frac{1+\cos\theta}{\cos\theta} \tag{6}$$

For a structured surface, if $\eta > \eta_e$, the composite state is more stable than the wetted state, and *vice versa*, which is related to a global minimum free Gibbs energy. Furthermore a critical hydraulic pressure was introduced. This quantitative study explains fairly well some experimental observations of contact angles that can be modeled neither by Wenzel nor Cassie–Baxter theory and eventually leads to proposals for a mixed (or coexisting) wetting mode.

There are many more models describe the transition states.[134–136] Most of models are based on analyzing the free energy or the pressure. Some models are very complex, thus are difficult to evaluate and to apply for surface analysis. Nevertheless, each model is based on certain assumptions, which would in principle give the model some inherent limits.

5 Applications

Applications of superhydrophobic surfaces are interesting because self-cleaning and antisticking properties of the surfaces are prominent.[4,25] These properties are desirable for many industrial and biological applications such as antibiofouling paints for boats,[14,15] antisticking of snow for antennas and windows,[16,17] self-cleaning windshields for automobiles,[18] metal refining, stain resistant textiles, antisoiling architectural coatings,[19] the separation of water and oil,[137] and in the textile industry such as in the manufacture of water-proof, fire-retardant clothes.[97,138–140]

Recently, antifouling behavior of superhydrophobic has been tested on a silica nanoparticles embedded in polysiloxane materials.[141] Comparison of the fouling behavior of a smooth polysiloxane polymer film and roughened superhydrophobic coatings revealed that the effect of nanoscale interfacial roughness is crucial as witnessed by the fact that micro-organism did not attach to the superhydrophobic surfaces in the first weeks of the fouling tests.

The superhydrophobic phenomenon known for long time, has been recognized and it has provoked a lot of research interests in the last decade mostly benefited from the fast progress in nanotechnology. The advantages of superhydrophobic surfaces are apparent, but before real applications come into our daily life some problems have to be solved or addressed.

Contamination

The naturally occurring superhydrophobic surfaces such as lotus leaves are living objects. The surfaces can be easily repaired or regenerated, for example, epicuticular wax is secreted by the leaf continuously. For man-made superhydrophobic surfaces, the water repellent capability gradually degrades during long-term outdoor exposure and accumulation of contamination. This problem was addressed by introduction of photocatalytic coatings, such as TiO_2[12] and apatite.[142] Both catalysts can oxidize organic stains under UV illumination. However, a drawback of TiO_2 is that the surface becomes superhydrophilic after the irradiation,[143] which has inherent higher affinity to stains. The apatite based catalyst does not transform the surface property under UV illumination, which seems promising.

Wear resistance

Wear resistance is an important issue in the application of superhydrophobic surfaces. The lotus leaf itself is very fragile in the micro- and nanostructures.[7] To make robust micro- and nanostructures is of key importance for the application of superhydrophobic surfaces. There are not many reports addressing this problem. Wu *et al.*[51] have used microwave plasma enhanced CVD to prepare superhydrophobic thin films starting from trimethylmethoxysilane (TMMOS). The mechanical properties of the resulting surfaces were tested. The wear resistance of the film was studied by AFM and mechanical durability was tested by rubbing the surface with flannel cloth under 200 g of load. It was found that the water repellent capability decreased and the contact angle dropped approximately 20°. However, the CA after initial decrease stayed stable even upon prolonged rubbing for 3000 times. These test conditions are relatively mild, depending on the nature of the application and more realistic tests should be

View Online

designed. Moreover, for surfaces with contact angle lower than 150°, the superhydrophobic state no longer exists.

Transparency

Optically transparent coatings will render superhydrophobic coatings versatile in applications such as microfluidic devices and biomedical devices. The problem has been recognized and addressed by many groups and a rich collection of materials have been used from silica to polymers.[12,49,61,83,94,113,121,144–149]

There are other issues, such as the requirements for substrate treatment, costly roughening procedures, and large area preparation, *etc*, that would hamper the application of superhydrophobic surfaces on a larger scale. However, in many high-tech applications, such as medical devices, these issues are not important. Examples of medical devices based on superhydrophobic surfaces have been reported.[150] In general, the preparation of superhydrophobic surfaces is still in its initial state. The procedures are mostly costly and sometimes lengthy with respect to the number of steps and surface treatments. However, as shown in section 3, many procedures have been developed, and many issues towards real life application have been recognized and addressed. Thus it is fair to say that the application of superhydrophobic surfaces to real life will be realistic in the future.

6 Conclusions

Many approaches have been used for the creation of superhydrophobic surfaces. Theoretical aspects predict that a combination of multiphases and a high roughness factor give the best results. Many approaches have been drawn up as discussed above and many controversies still exist as to what is the critical standard for the generation of superhydrophobic surfaces. Despite the theoretical conflicts, superhydrophobic surfaces are receiving more and more attention, and the potential applications are increasingly recognized. Benefiting from the advancing progress in micro- and nanofabrication techniques, diverse fabrication methods and a large variety of materials have been used, ranging from inorganic nanoparticles to bulk polymeric materials. This rich knowledge will be beneficial for the application of superhydrophobic surfaces in real life.

References

1 A. W. Adamson, *Physical Chemistry of Surfaces*, Wiley, New York, 1990.
2 S. Shibuichi, T. Onda, N. Satoh and K. Tsujii, *J. Phys. Chem.*, 1996, **100**, 19512.
3 I. P. Parkin and R. G. Palgrave, *J. Mater. Chem.*, 2005, **15**, 1689.
4 T. L. Sun, L. Feng, X. F. Gao and L. Jiang, *Acc. Chem. Res.*, 2005, **38**, 644.
5 J. De Coninck, M. J. de Ruijter and M. Voue, *Curr. Opin. Colloid Interface Sci.*, 2001, **6**, 49.
6 T. Onda, S. Shibuichi, N. Satoh and K. Tsujii, *Langmuir*, 1996, **12**, 2125.
7 W. Barthlott and C. Neinhuis, *Planta*, 1997, **202**, 1.
8 A. Lafuma and D. Quere, *Nat. Mater.*, 2003, **2**, 457.
9 R. Blossey, *Nat. Mater.*, 2003, **2**, 301.
10 R. Furstner, W. Barthlott, C. Neinhuis and P. Walzel, *Langmuir*, 2005, **21**, 956.
11 M. Miwa, A. Nakajima, A. Fujishima, K. Hashimoto and T. Watanabe, *Langmuir*, 2000, **16**, 5754.
12 A. Nakajima, K. Hashimoto, T. Watanabe, K. Takai, G. Yamauchi and A. Fujishima, *Langmuir*, 2000, **16**, 7044.
13 A. Otten and S. Herminghaus, *Langmuir*, 2004, **20**, 2405.
14 A. Scardino, R. De Nys, O. Ison, W. O'Connor and P. Steinberg, *Biofouling*, 2003, **19**, 221.
15 M. P. Schultz, C. J. Kavanagh and G. W. Swain, *Biofouling*, 1999, **13**, 323.
16 H. Saito, K. Takai, H. Takazawa and G. Yamauchi, *Mater. Sci. Res. Int.*, 1997, **3**, 216.
17 T. Kako, A. Nakajima, H. Irie, Z. Kato, K. Uematsu, T. Watanabe and K. Hashimoto, *J. Mater. Sci.*, 2004, **39**, 547.
18 D. Quere, *Rep. Prog. Phys.*, 2005, **68**, 2495.
19 M. Zielecka and E. Bujnowska, *Prog. Org. Coat.*, 2006, **55**, 160.
20 S. R. Coulson, I. Woodward, J. P. S. Badyal, S. A. Brewer and C. Willis, *J. Phys. Chem. B*, 2000, **104**, 8836.
21 T. Nishino, M. Meguro, K. Nakamae, M. Matsushita and Y. Ueda, *Langmuir*, 1999, **15**, 4321.
22 X. F. Gao and L. Jiang, *Nature*, 2004, **432**, 36.
23 W. Lee, M. K. Jin, W. C. Yoo and J. K. Lee, *Langmuir*, 2004, **20**, 7665.
24 D. Quere, *Physica A (Amsterdam)*, 2002, **313**, 32.
25 A. Nakajima, K. Hashimoto and T. Watanabe, *Monatsh. Chem.*, 2001, **132**, 31.
26 M. Callies and D. Quere, *Soft Matter*, 2005, **1**, 55.
27 J. B. Brzoska, I. Benazouz and F. Rondelez, *Langmuir*, 1994, **10**, 4367.
28 G. D. Nadkarni and S. Garoff, *Langmuir*, 1994, **10**, 1618.
29 R. N. Wenzel, *Ind. Eng. Chem.*, 1936, **28**, 988.
30 A. B. D. Cassie and S. Baxter, *Trans. Faraday Soc.*, 1944, **40**, 546.
31 Z. Yoshimitsu, A. Nakajima, T. Watanabe and K. Hashimoto, *Langmuir*, 2002, **18**, 5818.
32 V. Stelmashuk, H. Biederman, D. Slavinska, J. Zemek and M. Trchova, *Vacuum*, 2005, **77**, 131.
33 D. Oner and T. J. McCarthy, *Langmuir*, 2000, **16**, 7777.
34 S. H. Kim, J. H. Kim, B. K. Kang and H. S. Uhm, *Langmuir*, 2005, **21**, 12213.
35 M. Hikita, K. Tanaka, T. Nakamura, T. Kajiyama and A. Takahara, *Langmuir*, 2005, **21**, 7299.
36 J. Carpentier and G. Grundmeier, *Surf. Coat. Technol.*, 2005, **192**, 189.
37 J. Jopp, H. Grull and R. Yerushalmi-Rozen, *Langmuir*, 2004, **20**, 10015.
38 R. E. Johnson Jr. and R. H. Dettre, *Adv. Chem. Ser.*, 1963, **43**, 112.
39 C. Neinhuis and W. Barthlott, *Ann. Bot.*, 1997, **79**, 667.
40 E. A. Baker, *Chemistry and Morphology of Plant Epicuticular Waxes*, in *The Plant Cuticle, Linnean Society Symposium Series*, ed. D. F. Cutler, K. L. Alvin and C. E. Price, Academic Press, London, 1982.
41 C. E. Jeffree, *The Cuticle, Epicuticular Waxes and Trichomes of Plants, with Reference to their Structure, Functions and Evolution*, in *Insects and the Plant Surface*, ed. B. Juniper and R. Southwood, Edward Arnold, London, 1986.
42 M. H. Sun, C. X. Luo, L. P. Xu, H. Ji, O. Y. Qi, D. P. Yu and Y. Chen, *Langmuir*, 2005, **21**, 8978.
43 J. Li, J. Fu, Y. Cong, Y. Wu, L. J. Xue and Y. C. Han, *Appl. Surf. Sci.*, 2006, **252**, 2229.
44 J. Fresnais, L. Benyahia and F. Poncin-Epaillard, *Surf. Interface Anal.*, 2006, **38**, 144.
45 M. Kiuru and E. Alakoski, *Mater. Lett.*, 2004, **58**, 2213.
46 S. J. Lee, B. G. Paik, G. B. Kim and Y. G. Jang, *Jpn. J. Appl. Phys., Part 1*, 2006, **45**, 912.
47 J. Liang and B. Q. Liu, *Chinese J. Polym. Sci.*, 2005, **23**, 83.
48 D. O. H. Teare, C. G. Spanos, P. Ridley, E. J. Kinmond, V. Roucoules, J. P. S. Badyal, S. A. Brewer, S. Coulson and C. Willis, *Chem. Mater.*, 2002, **14**, 4566.
49 K. Teshima, H. Sugimura, Y. Inoue, O. Takai and A. Takano, *Appl. Surf. Sci.*, 2005, **244**, 619.
50 K. Teshima, H. Sugimura, Y. Inoue, O. Takai and A. Takano, *Chem. Vap. Deposition*, 2004, **10**, 295.
51 Y. Y. Wu, M. Bekke, Y. Inoue, H. Sugimura, H. Kitaguchi, C. S. Liu and O. Takai, *Thin Solid Films*, 2004, **457**, 122.
52 J. T. Han, Y. Zheng, J. H. Cho, X. Xu and K. Cho, *J. Phys. Chem. B*, 2005, **109**, 20773.

Published on 31 January 2007 on http://pubs.rsc.org | doi:10.1039/B602486F
Downloaded on 29 November 2010

 This journal is © The Royal Society of Chemistry 2007

View Online

Published on 31 January 2007 on http://pubs.rsc.org | doi:10.1039/B602486F
Downloaded on 29 November 2010

53 W. H. Jiang, G. J. Wang, Y. N. He, Y. L. An, X. G. Wang, Y. L. Song and L. Jiang, *Chem. J. Chinese Univ. (Chinese)*, 2005, **26**, 1360.
54 W. H. Jiang, G. J. Wang, Y. N. He, X. G. Wang, Y. L. An, Y. L. Song and L. Jiang, *Chem. Commun.*, 2005, 3550.
55 S. A. Kulinich and M. Farzaneh, *Surf. Sci.*, 2004, **573**, 379.
56 D. Schondelmaier, S. Cramm, R. Klingeler, J. Morenzin, C. Zilkens and W. Eberhardt, *Langmuir*, 2002, **18**, 6242.
57 T. Soeno, K. Inokuchi and S. Shiratori, *Appl. Surf. Sci.*, 2004, **237**, 543.
58 X. Y. Song, J. Zhai, Y. L. Wang and L. Jiang, *J. Phys. Chem. B*, 2005, **109**, 4048.
59 G. Zhang, D. Y. Wang, Z. Z. Gu and H. Mohwald, *Langmuir*, 2005, **21**, 9143.
60 N. Zhao, F. Shi, Z. Q. Wang and X. Zhang, *Langmuir*, 2005, **21**, 4713.
61 Y. Y. Wu, H. Sugimura, Y. Inoue and O. Takai, *Chem. Vap. Deposition*, 2002, **8**, 47.
62 F. Shi, Z. Q. Wang and X. Zhang, *Adv. Mater.*, 2005, **17**, 1005.
63 M. L. Ma, Y. Mao, M. Gupta, K. K. Gleason and G. C. Rutledge, *Macromolecules*, 2005, **38**, 9742.
64 H. Liu, L. Feng, J. Zhai, L. Jiang and D. B. Zhu, *Langmuir*, 2004, **20**, 5659.
65 M. Li, J. Zhai, H. Liu, Y. L. Song, L. Jiang and D. B. Zhu, *J. Phys. Chem. B*, 2003, **107**, 9954.
66 E. Honoso, S. Fujihara, I. Honma and H. Zhou, *J. Am. Chem. Soc.*, 2005, **127**, 13458.
67 J. T. Han, D. H. Lee, C. Y. Ryu and K. W. Cho, *J. Am. Chem. Soc.*, 2004, **126**, 4796.
68 P. L. Chen, *Abstr. Pap. Am. Chem. Soc.*, 2003, **226**, U382.
69 Y. Li, W. P. Cai, B. Q. Cao, G. T. Duan and F. Q. Sun, *Polymer*, 2005, **46**, 12033.
70 A. Nakajima, C. Saiki, K. Hashimoto and T. Watanabe, *J. Mater. Sci. Lett.*, 2001, **20**, 1975.
71 L. Jiang, Y. Zhao and J. Zhai, *Angew. Chem., Int. Ed.*, 2004, **43**, 4338.
72 Z. Z. Gu, H. M. Wei, R. Q. Zhang, G. Z. Han, C. Pan, H. Zhang, X. J. Tian and Z. M. Chen, *Appl. Phys. Lett.*, 2005, 86.
73 A. Singh, L. Steely and H. R. Allcock, *Langmuir*, 2005, **21**, 11604.
74 K. Acatay, E. Simsek, C. Ow-Yang and Y. Z. Menceloglu, *Angew. Chem., Int. Ed.*, 2004, **43**, 5210.
75 K. Y. Suh and S. Jon, *Langmuir*, 2005, **21**, 6836.
76 B. He, N. A. Patankar and J. Lee, *Langmuir*, 2003, **19**, 4999.
77 N. A. Patankar, *Langmuir*, 2004, **20**, 8209.
78 N. A. Patankar, *Langmuir*, 2004, **20**, 7097.
79 N. A. Patankar, *Langmuir*, 2003, **19**, 1249.
80 E. Martines, K. Seunarine, H. Morgan, N. Gadegaard, C. D. W. Wilkinson and M. O. Riehle, *Nano Lett.*, 2005, **5**, 2097.
81 M. H. Jin, X. J. Feng, L. Feng, T. L. Sun, J. Zhai, T. J. Li and L. Jiang, *Adv. Mater.*, 2005, **17**, 1977.
82 A. Nakajima, K. Abe, K. Hashimoto and T. Watanabe, *Thin Solid Films*, 2000, **376**, 140.
83 A. Nakajima, A. Fujishima, K. Hashimoto and T. Watanabe, *Adv. Mater.*, 1999, **11**, 1365.
84 S. Minko, M. Muller, M. Motornov, M. Nitschke, K. Grundke and M. Stamm, *J. Am. Chem. Soc.*, 2003, **125**, 3896.
85 M. T. Khorasani and H. Mirzadeh, *J. Appl. Polym. Sci.*, 2004, **91**, 2042.
86 M. T. Khorasani, H. Mirzadeh and Z. Kermani, *Appl. Surf. Sci.*, 2005, **242**, 339.
87 L. J. Guo, *J. Phys. D: Appl. Phys.*, 2004, **37**, R123.
88 K. Autumn, Y. A. Liang, S. T. Hsieh, W. Zesch, W. P. Chan, T. W. Kenny, R. Fearing and R. J. Full, *Nature*, 2000, **405**, 681.
89 L. Feng, Y. L. Song, J. Zhai, B. Q. Liu, J. Xu, L. Jiang and D. B. Zhu, *Angew. Chem., Int. Ed.*, 2003, **42**, 800.
90 G. Cicala, A. Milella, E. Palumbo, P. Favia and R. d'Agostino, *Diamond Relat. Mater.*, 2003, **12**, 2020.
91 Y. Y. Wu, M. Kuroda, H. Sugimura, Y. Inoue and O. Takai, *Surf. Coat. Technol.*, 2003, **174**, 867.
92 Y. Y. Wu, H. Sugimura, Y. Inoue and O. Takai, *Thin Solid Films*, 2003, **435**, 161.
93 W. A. Daoud, J. H. Xin and X. M. Tao, *J. Am. Ceram. Soc.*, 2004, **87**, 1782.
94 G. Gu, H. Dang, Z. Zhang and Z. Wu, *Appl. Phys. A: Mater. Sci. Process.*, 2006, **83**, 131.
95 D. H. Jung, I. J. Park, Y. K. Choi, S. B. Lee, H. S. Park and J. Ruhe, *Langmuir*, 2002, **18**, 6133.
96 X. H. Li, Z. Cao, F. Liu, Z. J. Zhang and H. X. Dang, *Chem. Lett.*, 2006, **35**, 94.
97 B. Mahltig and H. Bottcher, *J. Sol–Gel Sci. Technol.*, 2003, **27**, 43.
98 K. Makita, Y. Akamatsu, S. Yamazaki, Y. Kai and Y. Abe, *J. Ceram. Soc. Jpn.*, 1997, **105**, 1012.
99 T. Nakagawa and M. Soga, *J. Non-Cryst. Solids*, 1999, **260**, 167.
100 A. V. Rao, M. M. Kulkarni, D. P. Amalnerkar and T. Seth, *J. Non-Cryst. Solids*, 2003, **330**, 187.
101 A. V. Rao, G. M. Pajonk, S. D. Bhagat and P. Barboux, *J. Non-Cryst. Solids*, 2004, **350**, 216.
102 A. Roig, E. Molins, E. Rodriguez, S. Martinez, M. Moreno-Manas and A. Vallribera, *Chem. Commun.*, 2004, 2316.
103 N. J. Shirtcliffe, G. McHale, M. I. Newton and C. C. Perry, *Langmuir*, 2003, **19**, 5626.
104 S. Sosa, *MRS Bull.*, 2004, **29**, 910.
105 W. Ming, D. Wu, R. van Benthem and G. de With, *Nano Lett.*, 2005, **5**, 2298.
106 E. Hosono, S. Fujihara, I. Honma and H. S. Zhou, *J. Am. Chem. Soc.*, 2005, **127**, 13458.
107 X. D. Wu, L. J. Zheng and D. Wu, *Langmuir*, 2005, **21**, 2665.
108 L. Huang, S. P. Lau, H. Y. Yang, E. S. P. Leong, S. F. Yu and S. Prawer, *J. Phys. Chem. B*, 2005, **109**, 7746.
109 X. Zhang, F. Shi, X. Yu, H. Liu, Y. Fu, Z. Q. Wang, L. Jiang and X. Y. Li, *J. Am. Chem. Soc.*, 2004, **126**, 3064.
110 J. Y. Shiu, C. W. Kuo, P. L. Chen and C. Y. Mou, *Chem. Mater.*, 2004, **16**, 561.
111 L. Zhai, F. C. Cebeci, R. E. Cohen and M. F. Rubner, *Nano Lett.*, 2004, **4**, 1349.
112 R. M. Jisr, H. H. Rmaile and J. B. Schlenoff, *Angew. Chem., Int. Ed.*, 2005, **44**, 782.
113 H. M. Shang, Y. Wang, S. J. Limmer, T. P. Chou, K. Takahashi and G. Z. Cao, *Thin Solid Films*, 2005, **472**, 37.
114 D. A. Doshi, P. B. Shah, S. Singh, E. D. Branson, A. P. Malanoski, E. B. Watkins, J. Majewski, F. van Swol and C. J. Brinker, *Langmuir*, 2005, **21**, 7805.
115 T. Sun, G. J. Wang, H. Liu, L. Feng, L. Jiang and D. B. Zhu, *J. Am. Chem. Soc.*, 2003, **125**, 14996.
116 L. B. Zhu, Y. H. Xiu, J. W. Xu, P. A. Tamirisa, D. W. Hess and C. P. Wong, *Langmuir*, 2005, **21**, 11208.
117 M. Mulder, *Basic Principles of Membrane Technology*, Kluwer Academic, Dordrecht, 1991.
118 H. Y. Erbil, A. L. Demirel, Y. Avci and O. Mert, *Science*, 2003, **299**, 1377.
119 X. Y. Lu, J. L. Zhang, C. C. Zhang and Y. C. Han, *Macromol. Rapid Commun.*, 2005, **26**, 637.
120 Q. D. Xie, J. Xu, L. Feng, L. Jiang, W. H. Tang, X. D. Luo and C. C. Han, *Adv. Mater.*, 2004, **16**, 302.
121 H. Yabu and M. Shimomura, *Chem. Mater.*, 2005, **17**, 5231.
122 L. L. Vogelaar, R. G. H. Lammertink and M. Wessling, *Langmuir*, 2006, **22**, 3125.
123 N. Zhao, Q. D. Xie, L. H. Weng, S. Q. Wang, X. Y. Zhang and J. Xu, *Macromolecules*, 2005, **38**, 8996.
124 Q. D. Xie, G. Q. Fan, N. Zhao, X. L. Guo, J. Xu, J. Y. Dong, L. Y. Zhang, Y. J. Zhang and C. C. Han, *Adv. Mater.*, 2004, **16**, 1830.
125 J. T. Han, X. R. Xu and K. W. Cho, *Langmuir*, 2005, **21**, 6662.
126 Z. M. Huang, Y. Z. Zhang, M. Kotaki and S. Ramakrishna, *Composites Sci. Technol.*, 2003, **63**, 2223.
127 M. L. Ma, R. M. Hill, J. L. Lowery, S. V. Fridrikh and G. C. Rutledge, *Langmuir*, 2005, **21**, 5549.
128 J. Bico, C. Marzolin and D. Quere, *Europhys. Lett.*, 1999, **47**, 220.
129 M. Lundgren, N. L. Allan, T. Cosgrove and N. George, *Langmuir*, 2003, **19**, 7127.
130 C. W. Extrand, *Langmuir*, 2005, **21**, 10370.
131 Y. T. Cheng and D. E. Rodak, *Appl. Phys. Lett.*, 2005, 86.
132 M. Nosonovsky and B. Bhushan, *Microsyst. Technol.*, 2006, **12**, 231.
133 Q. S. Zheng, Y. Yu and Z. H. Zhao, *Langmuir*, 2005, **21**, 12207.
134 D. Bartolo, F. Bouamrirene, E. Verneuil, A. Buguin, P. Silberzan and S. Moulinet, *Europhys. Lett.*, 2006, **74**, 299.
135 A. Dupuis and J. M. Yeomans, *Langmuir*, 2005, **21**, 2624.
136 C. Ishino, K. Okumura and D. Quere, *Europhys. Lett.*, 2004, **68**, 419.

View Online

137 L. Feng, Z. Y. Zhang, Z. H. Mai, Y. M. Ma, B. Q. Liu, L. Jiang and D. B. Zhu, *Angew. Chem., Int. Ed.*, 2004, **43**, 2012.
138 A. E. Baillie, S. B. Warner and Q. G. Fan, *AATCC Rev.*, 2005, **5**, 35.
139 G. N. Ramaswamy, B. Soeharto, W. R. Goynes, A. Salame, A. Lambert, E. Blanchard, D. V. Parikh, B. J. Collier, I. Negelescu, Y. Chen, M. Romanoschi and S. Despa, *Text. Chem. Color.*, 1997, **29**, 22.
140 V. V. Veselov, O. V. Meteleva and M. V. Nemikhina, *Fibres Text. East. Eur.*, 2000, **8**, 66.
141 H. Zhang, R. Lamb and J. Lewis, *Sci. Technol. Adv. Mater.*, 2005, **6**, 236.
142 N. Yoshida, M. Takeuchi, T. Okura, H. Monma, M. Wakamura, H. Ohsaki and T. Watanabe, *Thin Solid Films*, 2006, **502**, 108.
143 K. Tadanaga, J. Morinaga, A. Matsuda and T. Minami, *Chem. Mater.*, 2000, **12**, 590.
144 N. Yoshida, Y. Abe, H. Shigeta, K. Takami, H. Osaki, T. Watanabe, K. Hashimoto and A. Nakajima, *J. Sol–Gel Sci. Technol.*, 2004, **31**, 195.
145 A. Nakajima, *J. Ceram. Soc. Jpn.*, 2004, **112**, 533.
146 K. Takeda, M. Sasaki, N. Kieda, K. Katayama, T. Kako, K. Hashimoto, T. Watanabe and A. Nakajima, *J. Mater. Sci. Lett.*, 2001, **20**, 2131.
147 A. Hozumi, H. Sekoguchi, N. Sugimoto and O. Takai, *Trans. Inst. Met. Finish.*, 1998, **76**, 51.
148 O. Takai, A. Hozumi and N. Sugimoto, *J. Non-Cryst. Solids*, 1997, **218**, 280.
149 A. Hozumi, H. Sekoguchi, N. Kakinoki and O. Takai, *J. Mater. Sci.*, 1997, **32**, 4253.
150 G. J. Toes, K. W. van Muiswinkel, W. van Oeveren, A. J. H. Suurmeijer, W. Timens, I. Stokroos and J. van den Dungen, *Biomaterials*, 2002, **23**, 255.

Published on 31 January 2007 on http://pubs.rsc.org | doi:10.1039/B602486F
Downloaded on 29 November 2010

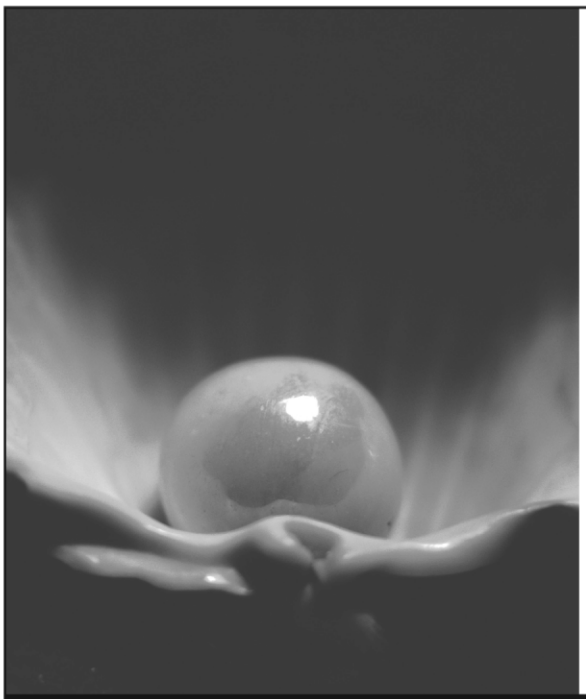

Looking for that **special** research paper from applied and technological aspects of the chemical sciences?

TRY this free news service:

Chemical Technology

- highlights of newsworthy and significant advances in chemical technology from across RSC journals
- free online access
- updated daily
- free access to the original research paper from every online article
- also available as a free print supplement in selected RSC journals.*

*A separately issued print subscription is also available.

Registered Charity Number: 207890

2205683

RSC Publishing

www.rsc.org/chemicaltechnology

This journal is © The Royal Society of Chemistry 2007